CHAPTER IV

RESULTS AND DISCUSSIONS

4.1 Introduction

This chapter discusses the results obtained from activities and experiments described in chapter III. Typical graphs related to the experimental works will be discussed in this chapter. Summarized results will be highlighted in appropriate tables and figures. Details of the experimental results are provided in Appendices. This chapter is divided into seven main sections, including preparation of biosorbent, evaluation of washing pre-treatment performance, advanced characterisation of biosorbent, optimisation of heavy metal biosorption, evaluation of existing model, application of biosorbent and development of ANN model. Sample analysis was conducted in duplicates and the data reported as average value with ± 1 SD as standard error. In general, the acquired data shows high reliability with less than 7 % probability of error. Since 97 % of the data obtained in this study have standard deviation less than 3 %, errors bars are not shown on the figures, but values are provided in the Appendices.

4.2 Preparation of Biosorbent

Three parameters for biosorbent preparation, namely, biosorbent concentration, immersion time and number of washing cycle were investigated.

4.2.1 Biosorbent Concentration

Figure 4.1 and Figure 4.2 show profiles of contaminants concentration leached-out per gram of biosorbent for light metal and heavy metal, respectively. These contaminants were detected for different biosorbent concentration in 200 mL UPW. These

concentrations represent the contaminants that had been leached out from biosorbent during the washing pre-treatment. The maximum contaminants concentration leached-out per gram of biosorbent was observed at 20 g/L biosorbent concentration. At this concentration, the biosorbent was easily wetted and settled to the bottom of beakers when left for two hours. When higher biosorbent concentrations were used, the volume of UPW (200 mL) was the limiting factor. The biosorbent was found to be partially wetted and tended to agglomerate, thus resulted in ineffective leaching of contaminants from the biosorbent. In designing subsequent experiments, 20 g/L biosorbent concentration was used in order to minimise UPW usage and optimise contaminants leaching from biosorbent.

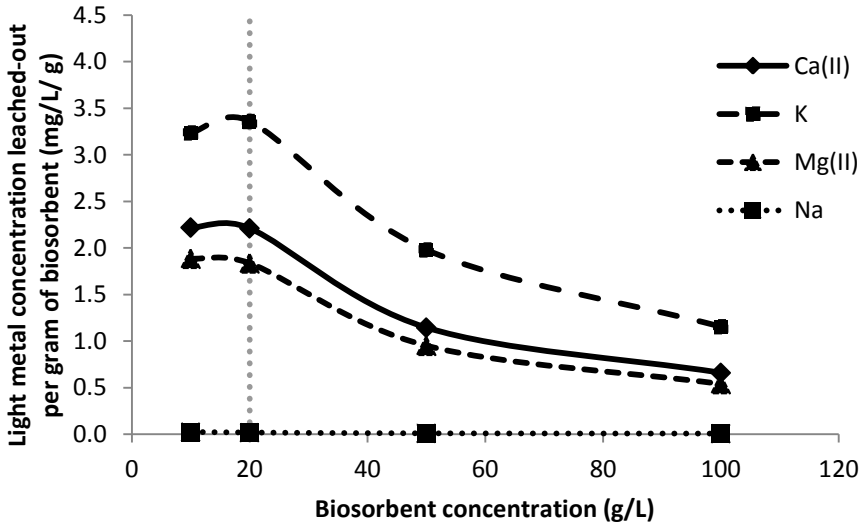

Figure 4.1 Light metal concentration per gram of biosorbent for different biosorbent concentration in 200 mL UPW

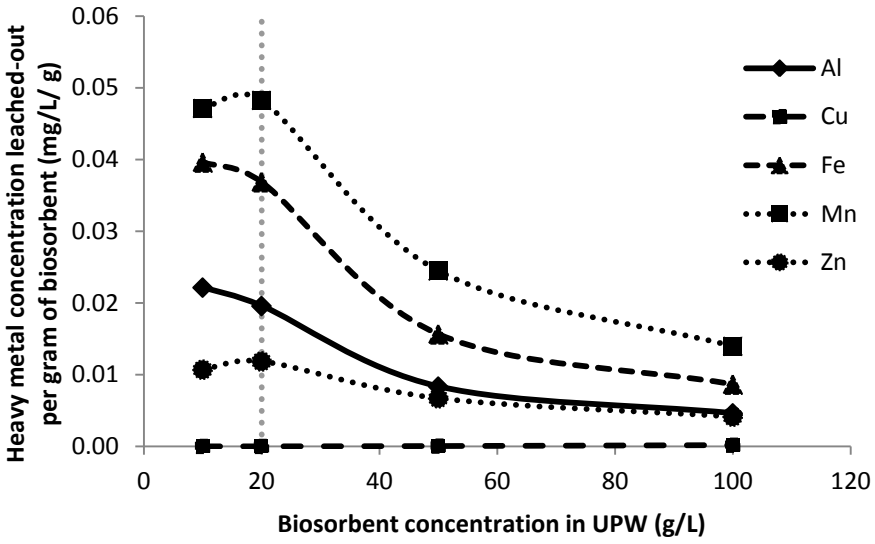

Figure 4.2 Heavy metal concentration per gram of biosorbent for different biosorbent concentration in 200 mL UPW

The light metal concentration leached-out per gram of biosorbent for potassium (K), calcium (Ca(II)), magnesium (Mg(II) and sodium (Na) were found to be 3.3578 ± 0.0011 mg/L, 2.2110 ± 0.0007 mg/L, 1.8348 ± 0.0053 mg/L and 0.0191 ± 0.0001 mg/L respectively. Leached K ions are possibly from the *Pleurotus ostreatus* mycelium as K ions are known to be the main electrolyte crucial to cellular transport (Caglarirmak, 2007). The concentration of Ca(II) and Mg(II) detected can be attributed to the use of natural limestone in the mushroom cultivation bag to maintain the pH of the substrate. Locally available limestone is dolomitic limestone which contains calcium and magnesium carbonates (Shamshuddin *et al*., 2009).

The concentrations of heavy metal leached-out per gram of biosorbent for manganese (Mn), ferum (Fe), aluminium (Al), zinc (Zn) and copper (Cu) were recorded at 0.0483 ± 0.0000 mg/L, 0.0369 ± 0.0002 mg/L, 0.0196 ± 0.0002 mg/L, 0.0119 ± 0.0001 mg/L and 0.0000 ± 0.0000 mg/L respectively. The source of heavy metal can be from the crushing and grinding process of sawdust using alloy steel blades. Core material of alloy steel comprises Fe, Mn and Al as they give good mechanical property (Bueno and Sordi,

2008), Zn improves the corrosion resistance (Ortiz *et al*., 2009) and Cu acts as contact reactive interlayer between Fe and Al (Wu *et al*., 2011). In addition, mineral content of mycelium biomass may also contribute to these heavy metals leached out from the biosorbent.

4.2.2 Immersion Time

Effect of immersion time on leaching out of the light and heavy metal contaminants concentration per gram of biosorbent is illustrated in Figure 4.3 and 4.4 respectively. The maximum contaminants concentration leached-out per gram of biosorbent was found at two hours immersion time. As immersion time increased, more biosorbent was wetted and contaminants were released into UPW, thus leading to significant increase in contaminants concentration leached-out per gram of biosorbent. While at longer immersion time, decrease in leached of contaminants was observed. This can be attributed to re-adsorption of contaminants into biosorbent. This indicates that contaminants can be removed effectively with an optimal immersion time of two hours. As the two hour immersion time represents the optimal immersion time, it was selected for following washing pre-treatment experimental design. It is worth to note that to date a study such as this has not been reported in the literature except for Reddad *et al*. (2002) and Entezari and Soltani (2009) where biosorbents were immersed in deionised water for twelve hours and two hours respectively.

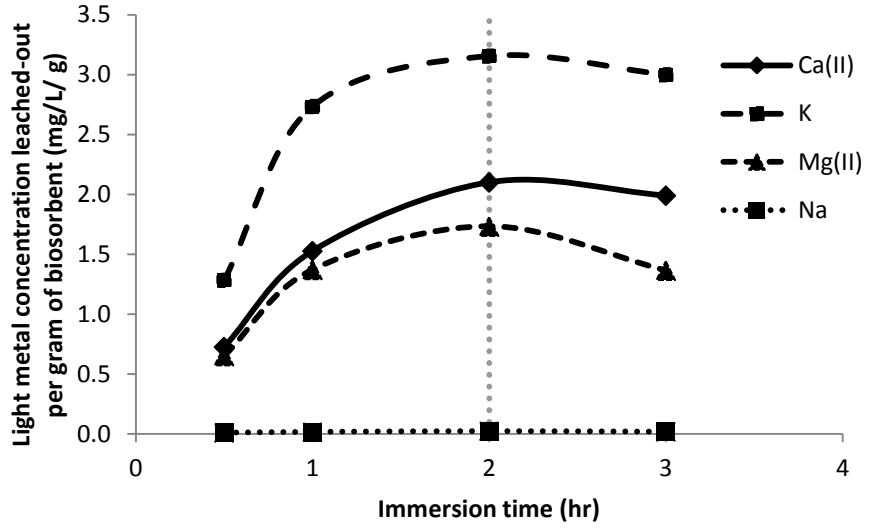

Figure 4.3 Light metal concentration per gram of biosorbent for different immersion time

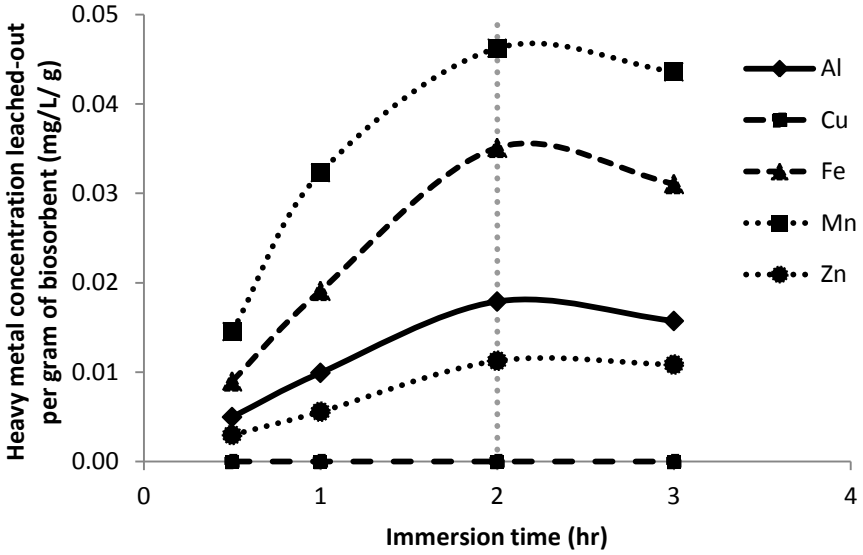

Figure 4.4 Heavy metal concentration per gram of biosorbent for different immersion time

The light metal concentration leached-out per gram of biosorbent was recorded at 3.1555 ± 0.0021 mg/L K, 2.1008 ± 0.0400 mg/L Ca(II), 1.7323 ± 0.0060 mg/L Mg(II) and 0.0241 ± 0.0001 mg/L Na. Meanwhile, the heavy metal concentration leached-out per gram of biosorbent were 0.0463 ± 0.0004 mg/L, 0.0351 ± 0.0002 mg/L, 0.0179 ± 0.0001 mg/L, 0.0113 ± 0.0000 mg/L and 0.0000 ± 0.0000 mg/L for Mn, Fe, Al, Zn and Cu respectively. These results are similar in trend as shown in Figure 4.1 and 4.2.

4.2.3 Number of Washing Cycle

Figures 4.5 and 4.6 depict percentage of contaminants removal for light metal and heavy metal detected for different number of washing cycle. When compared to first washing cycle, washing cycle two, three and four recorded a minimum contaminants removal of 60 ± 2.9463 %, 10 ± 2.5254 % and 7 ± 2.3149 % respectively. In addition, for washing cycle four, each light metal and heavy metal concentration per gram of biosorbent was less than 0.1000 mg/L and 0.0020 mg/L respectively. These infer that after three cycles of washing pre-treatment, contaminants has been almost completely removed. Therefore, three washing cycles of biosorbent washing pre-treatment was selected for subsequent experiments. Akar *et al*. (2009) documented that three washing cycle pre-treatment was carried out for silica gel immobilised biomass waste without any explanation.

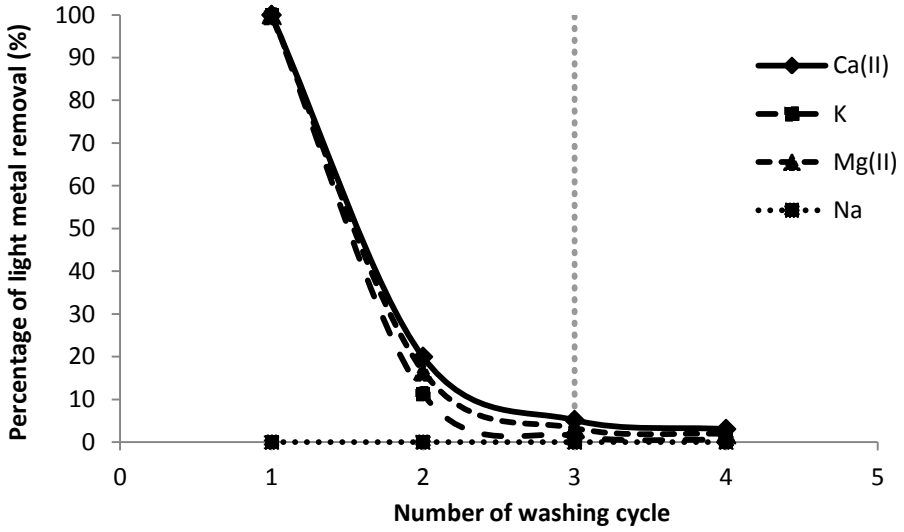

Figure 4.5 Percentage of light metal removal for different number of washing cycle

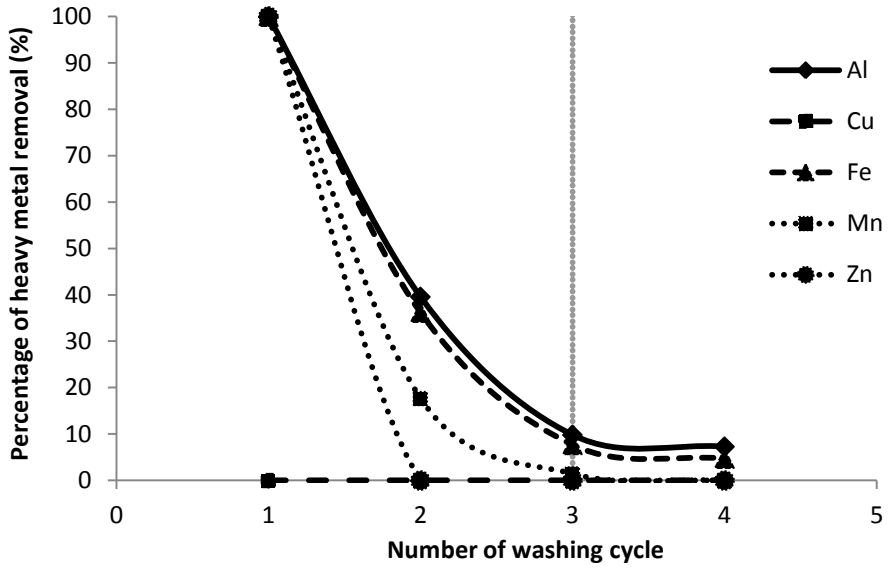

Figure 4.6 Percentage of heavy metal removal for different number of washing cycle

In summary, washing pre-treatment procedure in biosorbent preparation was examined. The optimal washing pre-treated PSMC conditions were 20 g/L of biosorbent concentration, two hours of immersion time and three cycles of washing pre-treatment. These results constitute a new approach for washing pre-treatment optimisation of biosorbent in biosorbent preparation. This approach not only minimises cost of washing pre-treatment but also time needed for effective washing pre-treatment and maximum leaching of contaminants from biosorbent.

4.3 Evaluation of Washing Pre-treatment Performance

The effect of washing pre-treatment on Ni(II) biosorption was examined. Reproducibility of biosorbent in batch mode preparation and repeatability of biosorption efficiency were investigated in order to evaluate washing pre-treatment performance.

4.3.1 The Effect of Washing Pre-treatment on Ni(II) Biosorption

Figure 4.7 shows the Ni(II) biosorption profiles for NW-PSMC and PSMC. A two-stage reaction which increased gradually and followed by a saturation stage was observed. As

the biosorbent concentration increased, the biosorption efficiency became noticeably different between NW-PSMC and PSMC. The saturation stage for Ni(II) biosorption was attained at 28.36 ± 0.09 % and 78.22 ± 0.03 % for NW-PSMC and PSMC respectively. Observation indicates that washing pre-treatment has removed the contaminants effectively and increased the active binding sites of biosorbent. Thus, this has increased Ni(II) biosorption performance by 50 %. This result emphasises the importance of washing pre-treatment in biosorbent preparation that reveals the biosorbent has good potential in heavy metal biosorption.

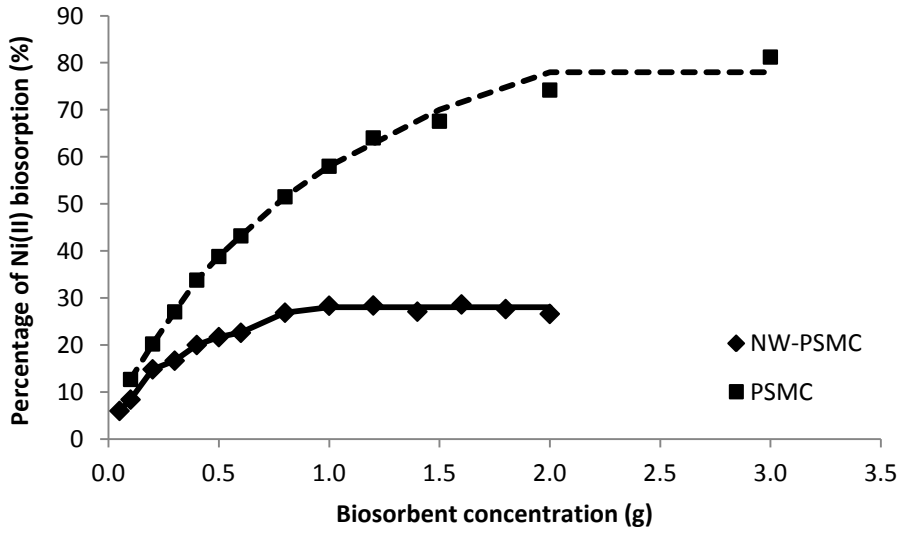

Figure 4.7 The effect of NW-PSMC and PSMC on Ni(II) biosorption efficiency

4.3.2 Reproducibility of Biosorbent and Repeatability of Ni(II) Biosorption

The performance of Ni(II) biosorption for five different batch of pre-treated biosorbent is shown in Table 4.1. The average of Ni(II) biosorption percentages of the five different batches of pre-treated biosorbent was found to be at 47.25 ± 1.18 %. The low variation in standard deviation results shows that the established washing pre-treatment methodology is consistent and reproducible for different batches of sampling. Furthermore, results also indicate that Ni(II) biosorption performance is consistent and reliable. Hence, investigation on the washing pre-treatment as conducted in this study is

a fundamental approach in method development for biosorbent preparation. This would contribute to improve the accuracy of results.

Table 4.1 Comparison study for reproducibility of biosorbent and repeatability of Ni(II) biosorption from batch to batch sampling

n	Ni(II) concentration (mg/L)				Ni(II) biosorption (%)			
	Co		*Ce*		1	2	Average	Std. dev.
	1	2	1	2				
1	54.78	54.22	28.65	28.09	47.70	48.19	47.95	0.35
2	51.24	50.44	27.87	27.89	45.61	44.71	45.16	0.64
3	54.41	54.50	28.08	28.60	48.39	47.52	47.96	0.61
4	53.66	53.54	27.88	28.30	48.04	47.14	47.59	0.64
5	51.24	50.44	29.30	28.98	48.04	47.14	47.59	0.64
Average							47.25	
Standard deviation							1.18	

In conclusion, the established washing pre-treatment process enhanced 50 % of Ni(II) biosorption from 28.36 ± 0.09 % to 78.22 ± 0.03 %. Evaluation on repeatability of Ni(II) biosorption from five different batches of washing pre-treated biosorbent showed excellent performance with low standard deviation value. Such results also indicate high reproducibility of washing pre-treated biosorbent in batch mode. Therefore, the established washing pre-treatment methodology is vital in cost-effectiveness calculation and biosorption performance that contribute towards sustainable remediation technology.

4.4 Advanced Characterisation of Biosorbent

The PSMC characterisation result is divided into three main parameters which included physical texture characterisation, chemical components characterisation and functional groups characterisation. These characterisations included BET surface area analysis, elemental analysis, cellulose and lignin analysis, SEM/EDX analysis, XPS analysis, zeta potential analysis, FTIR analysis and ^{13}C ssNMR analysis.

4.4.1 Brunauer Emmett Teller (BET) Surface Area Analysis

The surface area value (*aBET*) and mean apparent diameter (*dBET*) of PSMC biosorbent were found to be at 5.5544 x 10^{-1} m^2/g and 20.997 nm respectively. At the same time total pore volume (p/p_o = 0.990) of 2.9156 x 10^{-3} cm^3/g was measured. Table 4.2 compares the surface area and particle size of PSMC biosorbent with that reported in recent literature. The PSMC biosorbent with particle size ≤ 710 µm has a comparable surface area with other biosorbents except chemically modified magrove barks *Rhizophora apiculata*, marine algae *Posidonia oceanica* and fungus *Trametes versicolor*. Results give an indication that the PSMC physical biosorbent texture is a meso-porous biomaterial and has high surface area. These reveal that PSMC is a potential biosorbent for biosorption process. However, result needs to be investigated and confirmed by SEM analysis.

Table 4.2 Comparison of surface area and particle size PSMC with other recent reported studies

Biosorbent	Surface area (m^2/g)	Particle size (µm)	Reference(s)
Sawdust	1.96	211-422	Meena *et al*., 2008
Algae *Scenedesmus quadricauda* entrapped in Ca-alginate beads	0.97	2000	Bayramoğlu and Yakup Arıca, 2009
Waste pomace of olive oil factory	1.24	150-250	Nuhoglu and Malkoc, 2009
Modified quebracho tannin resin	0.820	34-53	Yurtsever and Şengil, 2009
Marine algae *Posidonia oceanica*	3.1	500-2000	Izquierdo *et al*., 2010
Chemically modified mangrove barks *Rhizophora apiculata*	3.453	250	Rozaini *et al*., 2010
Chitosan and chitosan derivatives beads	0.2903-0.4091	≤ 200	Ngah and Fatinathan, 2010
Sisal fiber *Agave sisalana*	0.0233	152	dos Santos *et al*., 2011
Fungus *Trametes versicolor*	3.103	200-300	Subbaiah *et al*., 2011a
PSMC	**0.55544**	**≤ 710**	**This study**

4.4.2 Elemental Analysis

Table 4.3 compares the elemental composition of PSMC biosorbent with other biosorbents that has been reported in the literature. With the exception of lignin, the amount of carbon in PSMC is quite similar to other biosorbents whereas the hydrogen content is similar with other studies except pecan nutshell. It can be inferred that cellulose seems to be the major component for PSMC biosorbent. PSMC has one order of magnitude lower concentration of nitrogen and sulphur when compared to modified baggase with amidoxime groups and lignin respectively. This reveals that PSMC biosorbent has low chitin and protein coumpounds. The relatively high amount of oxygen implies the possible presence of carboxyl functional group in PSMC. In general, carboxyl functional group consists of a carbonyl and a hydroxyl. These results require further investigation through other characterisations analysis.

Table 4.3 Comparison of elemental analysis of PSMC with relevant biosorbents

Biosorbent	C (%)	H (%)	N (%)	S (%)	O (%)	Reference
Industrial waste fungus biomass	48.0	7.6	4.4	-	-	Svecora *et al*., 2006
Lignin	60.8	5.8	1.3	2.1	-	Wu *et al*., 2008
Pecan nutshell	48.72	12.17	1.39	-	-	Vaghetti *et al*., 2009
Modified baggase (amidoxime groups)	43.96	7.13	13.64	-	-	Jiang *et al*., 2009
Marine green algae *Posidonia oceanica*	33.89	4.68	0.93	0.18	-	Izquierdo *et al*., 2010
Moringa oleifera bark	44.8	5.9	0.8	0.9	47.6	Reddy *et al*., 2011
Pleurotus ostreatus	44.10	5.60	5.20	0.2	45.10	Tay *et al*., 2011a
PSMC	**44.03**	**5.78**	**1.0**	**0.1**	**49.90**	**This study**

- Not available

4.4.3 Cellulose and Lignin Analysis

Results of cellulose and lignin analysis are shown in Table 4.4. The cellulosic content constitutes 73.6 ± 0.58 % holocellulose and 39.2 ± 0.36 % alpha-cellulose whilst the lignin content was only 13.8 ± 0.08 %. Low standard deviations indicate that the biosorbent is uniform and consistent in term s of lignocellulosic content.

Table 4.4 Cellulose and lignin content analysis

Description	Unit	Test method	Average	Std. dev.
Holocellulose content	%	Wise *et al.*, 1946	73.6	0.58
Alpha-cellulose content	%	TAPPI stamdard T203 cm-09: Alpha-, beta- and gamma-cellulose in pulp, 2009	39.2	0.36
Lignin content	%	TAPPI standard T222 om-02: Acid-insoluble lignin in wood and pulp, 2002	13.8	0.08

4.4.4 Scanning Electron Microscope/Energy Dispersive X-ray Spectroscopy (SEM/EDX) Analysis

Figure 4.8(a) depicts the heterogeneous, rough and porous surface of the biosorbent. It also shows that the external surface was full of cavity, suggesting the biosorbent has a high surface area. This porous characteristic of biosorbent facilitates the heavy metal ions diffusion and biosorption by reducing the diffusion resistance and mass transfer. Figure 4.8(b-d) illustrates slightly morphology changes with “muddy” deposit after heavy metal biosorption. These slight changes can be due to the chemisorptions processes and sudden changes in external bulk fluid environment, which can have a significant impact on its morphology.

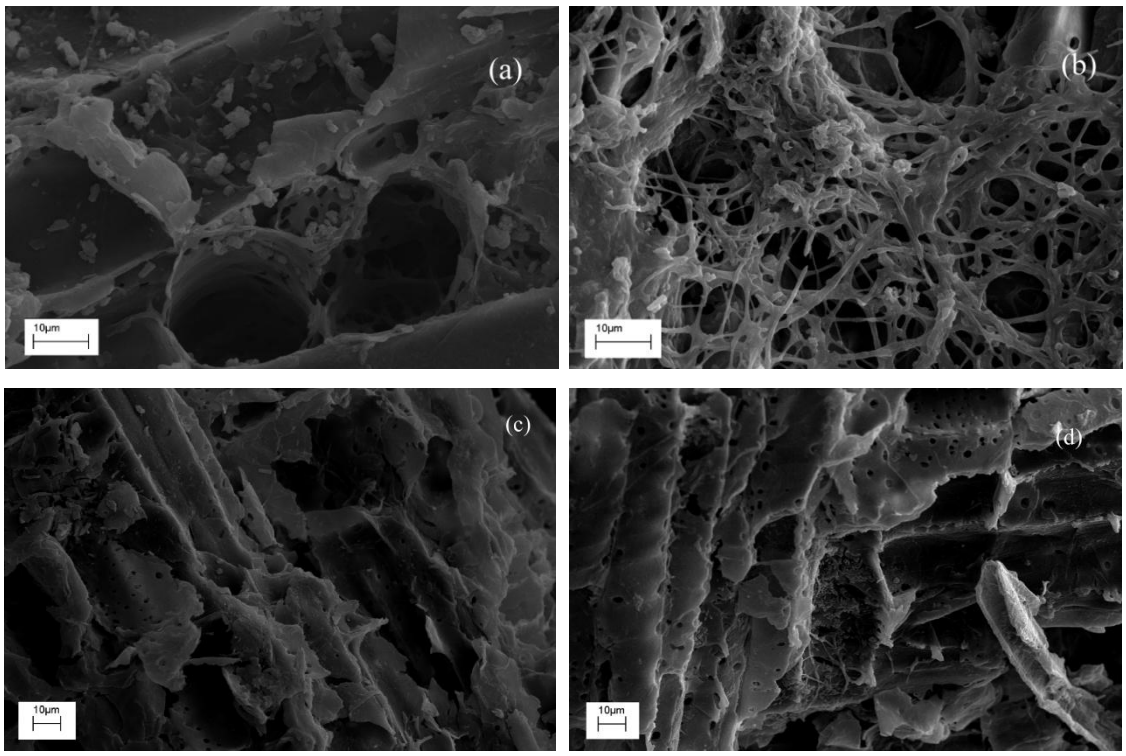

Figure 4.8 SEM micrograph of PSMC (a) before biosorption; (b) after Pb(II) biosorption; (c) after Cu(II) biosorption; and (d) after Ni(II) biosorption

Figure 4.9 illustrates the EDX spectra before and after heavy metal biosorption. Obvious peaks of C and O in EDX spectra supported the result from elemental analysis. The EDX analysis identified the peak of Mg(II) in the PSMC, that was not detected after the biosorption process. As expected, the heavy metal peaks were detected after biosorption process, which signify the attachment of heavy metal ions onto PSMC biosorbent. The disappearance of light metal Mg(II) peak and the presence of heavy metal peaks as revealed by EDX indicated the occurrence of ion exchange during biosorption process. Similar observation also has been reported by Tay *et al*. (2011a) and other researchers (Bueno *et al*., 2008; Mata *et al*., 2008; Qaiser *et al*., 2009; Kamal *et al*., 2010).

EDX analysis also quantifies the amount of metals in terms elemental and atomic percentages. However, these data were not presented as the EDX analysis conducted

was based on a random selection of selected areas and these semi-quantitative data may not represent the actual situation observed.

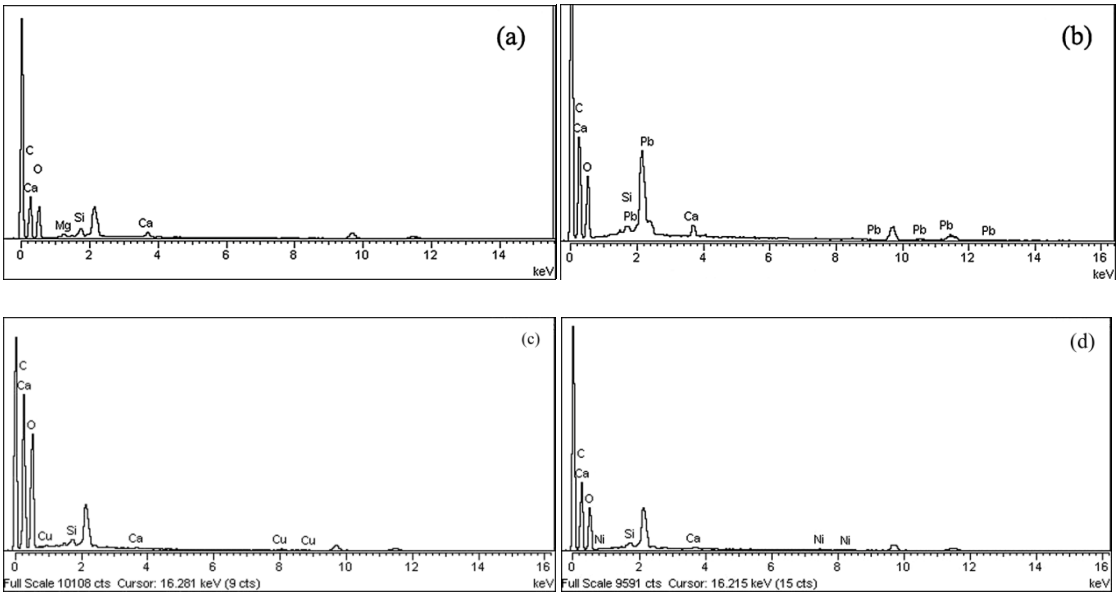

Figure 4.9 EDX spectrum of PSMC (a) before biosorption; (b) after Pb(II) biosorption; (c) after Cu(II) biosorption; and (d) after Ni(II) biosorption

4.4.5 X-ray Photoelectron Spectrometer (XPS) Analysis

Knowledge on electron configuration (1s, 2s, 2p, 3s, 3p, 4s, 3d, 4p, 5s, 4d) in atomic physics and quantum chemistry are applied to study the molecular orbital states within the biosorbent. Shifts of binding energy of the respective coordination atom in XPS deconvoluted spectra before and after heavy metal biosorption are shown in Table 4.5. In addition, Table 4.5 also shows recent studies which had the same findings. The samples before heavy metal biosorption indicate that carboxyl, hydroxyl from ether and alcohol as well as amide groups were present in lignocellulosic based PSMC biosorbent. This result provides an indication that the acidic groups of carboxyl, hydroxyl and amide, are functional groups involve in heavy metal biosorption.

Table 4.5 Identification of functional groups of PSMC biosorbent by XPS analysis

Valence state	Binding energy, BE (eV)				Identified functional groups	Reference(s)
	Before biosorption	After Pb(II) biosorption	After Cu(II) biosorption	After Ni(II) biosorption		
Carbon C 1s	286.177	286.244	286.134	286.244	C-O (hydroxyl of ether, alcohol) C=O (Carboxyl),	Lim *et al*., 2008; Murphy *et al*., 2009
	287.670	-	-	-	keto-enolic, iono-radical equilibria (C-O in the free-radical semiquinone group, carboxylo-carbonate ionic species)	Pakula *et al*., 1998; Lim *et al*., 2008; Ghods *et al*., 2011
Oxygen O 1s	531.542	-	-	-	C=O (carboxyl)	Lim *et al*., 2008
	532.510	532.248	532.221	532.276	COO^-	Chen *et al*., 2002
	533.414	532.963	533.029	533.020	H_2O	Moulder *et al*., 1992; Xi *et al*., 2010
Nitrogen N 1s	398.793	398.967	399.626	399.714	$H_2N(CH_2)_3COOH$ (amide)	Moulder *et al*., 1992; Beccari *et al*., 2009
Calcium Ca 2p $_{(3/2)}$	346.461	-	-	-	$CaCO_3$	Demri and Muster, 1995; Ghods *et al*., 2011
Lead Pb 4f $_{(7/2)}$		135.996			O-Pb-O of $Pb(OH)_2$ → Pb(II)	Chen *et al*., 2002
Copper Cu 2p $_{(3/2)}$	-		932.464		Alginate –bond Cu(II) → Cu(II)	Cheng *et al*., 2000; Naghash *et al*., 2006
Nickel Ni 2p $_{(3/2)}$				856.204	$Ni(OH)_2$ → Ni(II)	Nesbitt *et al*., 2000; Naghash *et al*., 2006

- Not detected

After heavy metal biosorption, it was observed that carboxyl peak of C 1s and O 1s were absent. The shift of nitrogen N 1s after heavy metal biosorption is assigned to amide group of organic nitrogen compound. These indicated that carboxyl from lignocellulosic and amide from chitin of *Pleurotus ostreatus* mycelia, were the major functional groups and components in heavy metal biosorption. Figueira *et al*. (1999) and Chen *et al*. (2002) also described that carboxyl group was involved in the biosorption process. These findings are consistent with the study conducted by Dizhbite *et al*. (1999) where nitrogen–containing derivatives and lignin were found to be promising biosorbent for heavy metal biosorption.

It was also observed that the calcium Ca 2p peak disappeared after heavy metal biosorption. This result revealed that the replacement of light metal by heavy metal ions is through an ion exchange mechanism. Canabady-Rochelle *et al*. (2010) through their investigation explained that Ca(II) ions would interact through electrostatic interactions rather than covalent interactions. In a separate study, Zvinowanda *et al*. (2010) reported that high quantities of light metal in *Zea Mays* tassel biosorbent are easily replaced by heavy metal that have low lying *d* and *f* orbitals. The sites on biosorbent surface holding these exchangeable light metal ions can then act as heavy metal binding sites for ion exchange mechanism.

The peak of Pb 4f, Cu 2p and Ni 2p were observed after heavy metal biosorption. These peaks were assigned to Pb(II), Cu(II) and Ni(II). Such observation provided evidence that there are no changes in heavy metal oxidation state of 2+ before and after biosorption process. These peaks may be ascribed to heavy metal ions combining with two oxygen containing groups through complexation. However, further investigations

through the use of FTIR and ^{13}C ssNMR were conducted to confirm the identified functional groups and proposed biosorption mechanism.

4.4.6 Zeta Potential Analysis

Zeta potential was investigated as a function of pH for PSMC biosorbent. Figure 4.10 illustrates a two phase reaction of zeta potential, starting with a decrease phase and then plateau. When pH increased, PSMC showed a significant increase in negative charge of zeta potential and this corresponded to the biosorption efficiency. This phenomenon indicates that the Van der Waals attraction between PSMC is stronger than the repulsive force between PSMC biosorbent and UPW. It can be concluded that an increase surface charge density on biosorbent at less acidic condition translates to a higher negative zeta potential, thus resulting in increase of biosorption performance. On the other hand, observation on higher pH at plateau phase was not applicable for Pb(II), Cu(II) and Ni(II). This is attributed to precipitation of Pb(II) and Cu(II) occurred above pH 5 as well as Ni(II) above pH 6. Therefore, the surface charge characteristics of PSMC in different initial pH conditions are corresponded with heavy metal biosorption efficiency. The isoelectric point that expected to fall in between pH 1 – 2 was not provided in this study as industrial wastewater in Malaysia is always in the range of pH 3 – 5 and pH 1 - 2 does not represent realistic operational condition for the biosorbent. Southichak *et al*. (2006) and Shin *et al*. (2007) reported a similar trend of observation in plant based biosorbents. In addition, this observation suggests that the weak acidic functional groups such as carboxyl, hydroxyl and amide interact with heavy metal during biosorption process. However, this needs to be investigated and supported using FTIR chatacterisation methods.

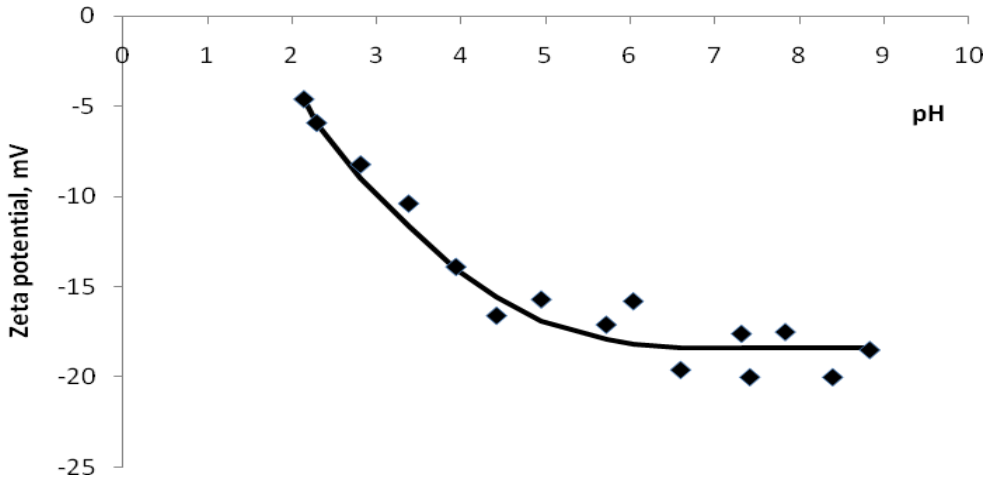

Figure 4.10 Zeta potential of PSMC biosorbent as a function of initial pH of the liquid medium

4.4.7 Fourier Transform Infrared Spectrometry (FTIR) Analysis

The characteristic bands present in lignocellulose, chitin and proteins obtained from the FTIR spectra are illustrated in Figure 4.11 and Table 4.6. In addition, Table 4.6 also shows recent studies with similar findings. The shifts of spectra summarized in Table 4.5 attests the fact that the carboxyl, hydroxyl and amide functional groups play a prominent role in heavy metal biosorption.

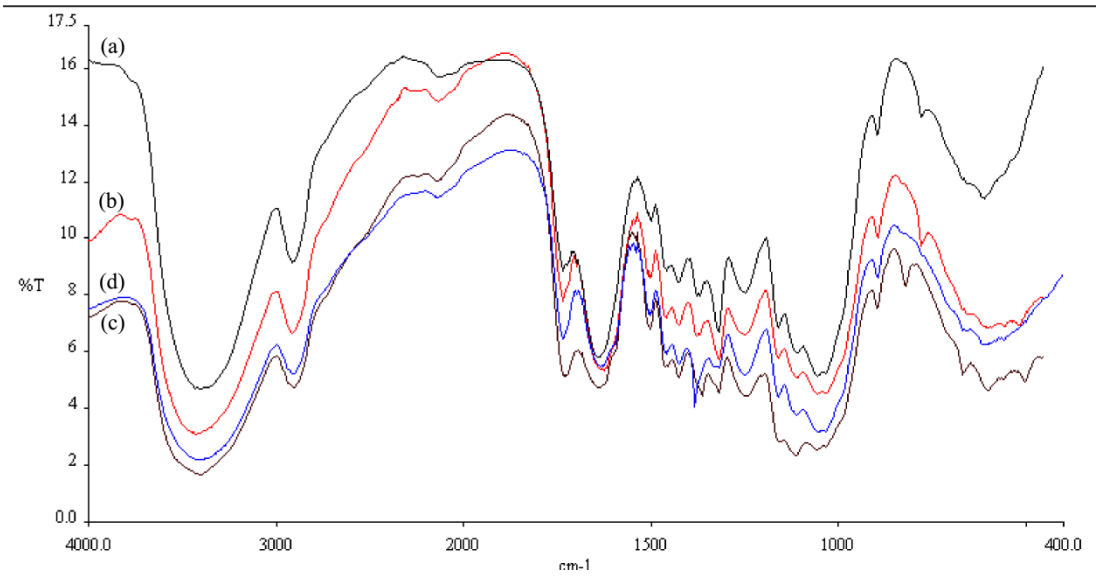

Figure 4.11 FTIR spectrum of PSMC biosorbent (a) before biosorption; (b) after Pb(II) biosorption; (c) after Cu(II) biosorption; and (d) after Ni(II) biosorption

Table 4.6 Identification of specific functional groups in PSMC biosorbent by FITR analysis

Wavelength number (cm^{-1})					
Before biosorption	After Pb(II) biosorption	After Cu (II) biosorption	After Ni(II) biosorption	Identified groups	Reference(s)
3400	3435	3401	3409	Bonded-OH or -NH stretching	Cayllahua *et al*., 2009; Luo *et al*., 2010; Munagapati *et al*., 2010; Subbaiah *et al*., 2011b
1640	1624	1642	1637	Asymmetric C=O, amide bend	Akmar Zakaria *et al*., 2009; Martín-Lara *et al*., 2010; Ramrakhiani *et al*., 2011; Xiao *et al*., 2010; Yang *et al*., 2011
1321/1371	1319/1371	1322/1371	1321/1384	C-O stretching of COOH or -CN groups	Naiya *et al*., 2009; Barka *et al*., 2010; Wahab *et al*., 2010; Reddy *et al*., 2011
1060/1111	1058/1111	1060/1116	1056/1111	C-O stretching of –OH and COOH	Li *et al*., 2010; Cruz-Olivares *et al*., 2011; Ji *et al*., 2011; Yipmantin *et al*., 2011
612	605	605	608	N-containing bioligands or -CN stretching	Vinodhini and Das, 2009; Barka *et al*., 2010

The peaks at 1640 cm^{-1}, 1321/1371cm^{-1} and 1060/1111 cm^{-1} were shifted after heavy metal biosorption. These suggest that the free carboxyl groups have changed into carboxylate, a phenomenon which normally occurs during the reaction between heavy metal and a carboxyl group. The identified carboxyl group, i. e., weak acidic functional groups confirms the XPS and zeta potential results. Chen *et al*. (2008) and Akmar Zakaria *et al*. (2009) noted that carboxyl is the main functional groups in heavy metal biosorption process for fungus *Lentinus edodes* and rubber tree sawdust respectively.

Pleurotus ostreatus, like any higher fungi, contains cell walls that contain chitin molecules (Ginterova and Maxiaitová, 1975). Vibrations at 3400 cm^{-1}, 1321/1371 cm^{-1} and 612 cm^{-1} of hydroxyl and amide groups, can be attributed to chitin. The identified functional groups of –OH, -NH and –CN provides further verification to support the presence of *Pleurotus ostreatus* mycelia in the biosorbent since these groups are characteristics of N-acetyl glucosamine that is the basic monomer for chitin. Bhanoori and Venkateswerlu (2000) reported that the oxygen ring and hydroxyl groups of N-acetyl glucosamine plays a significant role in binding with heavy metal ions via complexation through intra-molecular and inter-molecular interactions. In short, the identified hydroxyl and amide groups from organic nitrogen compounds of chitin concur with the result of XPS. This infers that it is a principal contributor in the chitin-heavy metal complexes. Li *et al*. (2010) and Tay *et al*. (2011b) suggested that, based on variations of the bands, FTIR spectra peaks indicate the prevalence of chelating characteristics of heavy metal biosorption through complexation mechanism. For amide functional group, it tends to form metal amide complexes via chelation.

It can be concluded that characterisation analysis using XPS and FTIR support that the carboxyl, hydroxyl and amide were the functional groups involved in heavy metal

biosorption with possibility of complexation mechanism. However, further investigation through the use of ^{13}C ssNMR was conducted to substantiate this observation, particularly for carboxyl group which found in lignocellulosic compound.

4.4.8 ^{13}C Solid State Nuclear Magnetic Resonance (^{13}C ssNMR) Analysis

Four types of ^{13}C ssNMR experiments, namely, CPMAS, DP SatRec, DP Invrec and TORCHIA were conducted to determine the functional groups and components involve in heavy metal biosorption as well as biosorption complexation mechanism.

4.4.8.1 Cross polarization (CPMAS)

Comparison between PSMC biosorbent before and after heavy metal biosorption process is depicted in Figure 4.12. There were no significant differences in the ^{13}C anisotropic chemical shift before and after heavy metal biosorption. This observation is attributed to the similar matrix of biosorbent and the signal filtering effects on CPMAS experimental design. The CPMAS involves magnetization transfer by hetero-nuclear dipolar coupling, thus suppressing signals from molecules moving with motional rates in the 8 kHz range. Therefore, further investigation on DP SatRec may help to explain this observation.

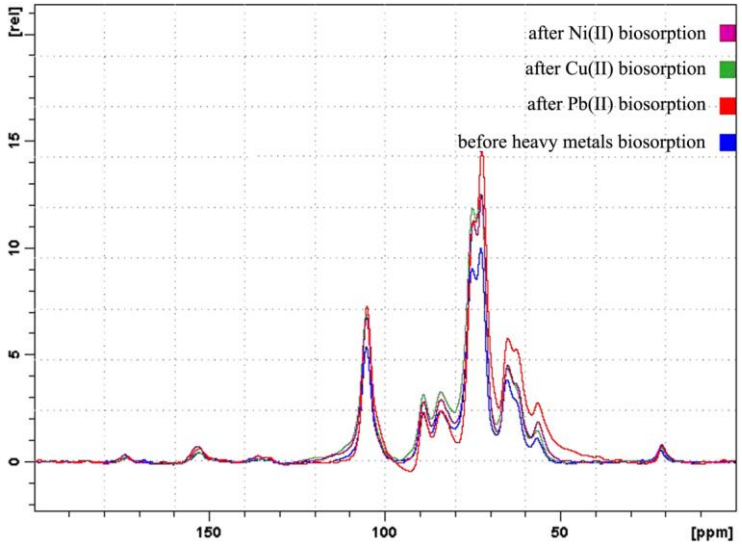

Figure 4.12 Comparisan of CPMAS spectra for PSMC biosorbent before and after heavy metal biosorption

Table 4.7 summarizes the general signals assignments of the ^{13}C CPMAS spectra for PSMC biosorbent. This result supports the fact that cellulose and lignin were major components found in PSMC biosorbent. The carboxyl and hydroxyl were present as surface functional groups of the lignocellulosic based biosorbent.

Table 4.7 The biosorbent functional groups and components from ^{13}C chemical shifts

No.	^{13}C chemical shifts, ppm	Signal type	Assignment of functional group for wood and lignin based materials
1	21.4	CH_3	CH_3COO^- in hemicelluloses
2	56.5	CH_3	-OCH_3 in hemicellulose Ar-OCH_3 in lignin
3	65.0	CH_2	C-6 in cellulose
	72.5	CH	C-2 - C-5 in cellulose and hemicellulose
	75.1	CH	C-2 - C-5 in cellulose and hemicellulose
	84.2	CH	C-4 in cellulose
	89.2	CH	C-4 in cellulose
4	105.2	CH	C-1 in cellulose
5	135.4	aromatic	C-1/C-4 of aromatic units in lignin of syringyl or guaiacyl
6	152.9	aromatic	C-1/C-3 in esterified and non-esterified syringyl units in lignin (carboxyl and hydroxyl compounds)
8	173.3	carboxyl	C=O in lignin (carboxyl compound)

(Hatfield *et al*., 1987; Neto *et al*., 1995; Bardet *et al*., 2002)

4.4.8.2 Direct pulse saturation recovery (DP SatRec)

Figure 4.13 illustrates the spectra of direct pulse saturation recovery, ^{13}C ssNMR for PSMC before and after heavy metal biosorption. Most of the ^{13}C signal is directly measured after excitation. These spectra showed less filtering effect if compared to

Figure 4.12. However, the result did not show significant changes in chemical shift before and after heavy metal biosorption although experiments took longer time due to very weak magnetization at the extreme tail of the free induction decay (FID). It turned out that the main concern for direct detection of the ^{13}C signal is signal-to-noise rather than resolution. These indicate that there is a need to use a new approach to determine the effect of heavy metal before and after biosorption process rather than using the conventional methods. First and foremost, experiments need to proceed with ^{1}H of DP Invrec to investigate paramagnetic effect of the heavy metal ions in ^{13}C ssNMR.

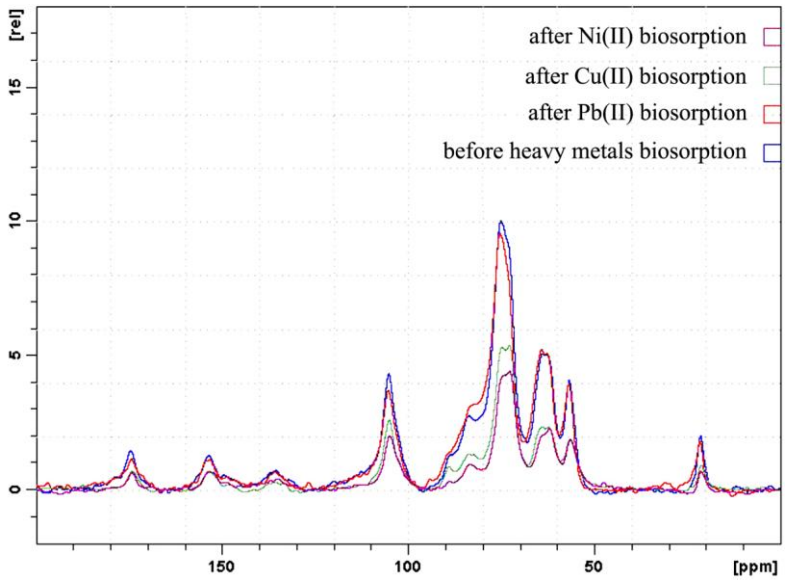

Figure 4.13 ^{13}C ssNMR spectra of DP SatRec before and after heavy metal biosorption

4.4.8.3 Direct pulse inversion recovery (DP Invrec)

The ^{1}H of DP Invrec is commonly used to investigate heavy metal ions that exhibit para-magnetic effect in ^{13}C ssNMR. Figure 4.14 shows DP Invrec experiments for Pb(II), Cu(II) and Ni(II). Pb(II) ions did not have paramagnetic effect. However, noticeable paramagnetic effects were observed on Cu(II) and Ni(II) samples ($\geq$ 0.05 mg/g) through ^{1}H proton analysis. Therefore, it is not possible to separate the effects of paramagnetic atoms apart in these samples. Further ^{13}C ssNMR approach for heavy metal biosorption evaluation on functional groups and mechanism were only conducted for Pb(II) as nuclear paramagnetism does not affects results.

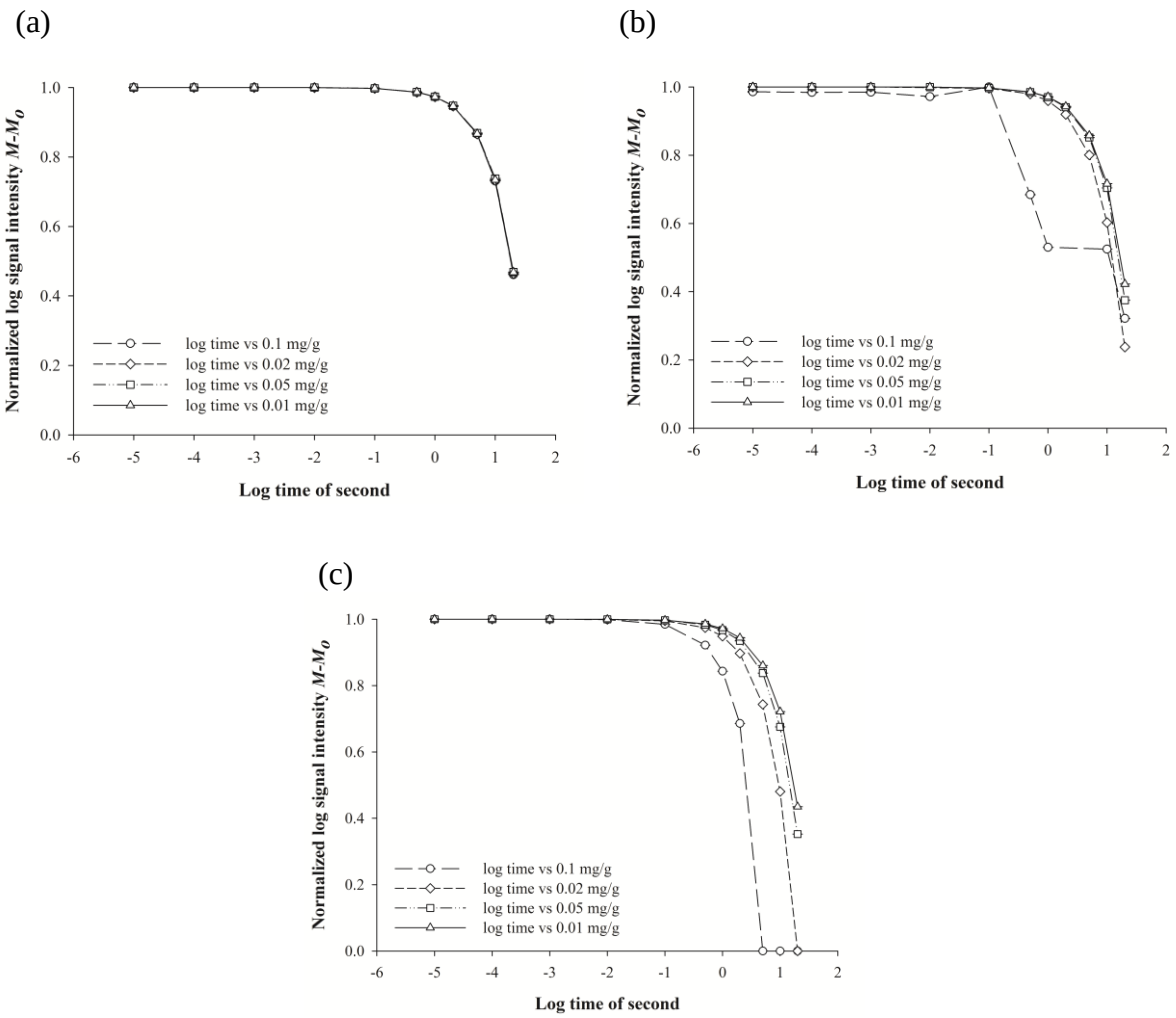

Figure 4.14 DP Invrec experiment for heavy metal ions paramagnetic effect evaluation (a) Pb(II); (b) Cu(II); and (c) Ni(II)

4.4.8.4 TORCHIA

TORCHIA experimental design is a novel approach introduced to evaluate mechanism of Pb(II) biosorption via functional groups determination. As previously explained, experiments were not conducted for Cu(II) and Ni(II) experiments due to their paramagnetic effect that interfere with the results. Figure 4.15 depicts the structural changes that occurred on lignin carboxyl and lignin C-1/C-4 of aromatic units of syringyl and guaiacyl for PSMC after Pb(II) biosorption process. Longer T_1 of PSMC after Pb(II) biosorption sample indicated that the sample had undergone "stiffening", i.e., the sample becomes more rigid. This is possibly ascribed to the formation of complexes. In TORCHIA experiments, the decrease in mobility of molecules with

longer T_1 infers the structural changes of molecules which play a pivotal role in complexation. The results obtained from ^{13}C ssNMR analysis was integratedly analysed with the results of XPS and FTIR analysis that lead to the confirmation of complexation between the Pb(II) and the carbonyl of the carboxylic functional group.

(a)

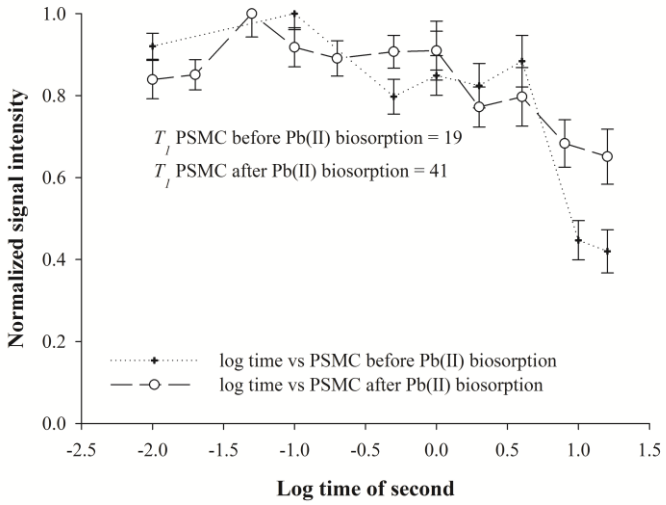

(b)

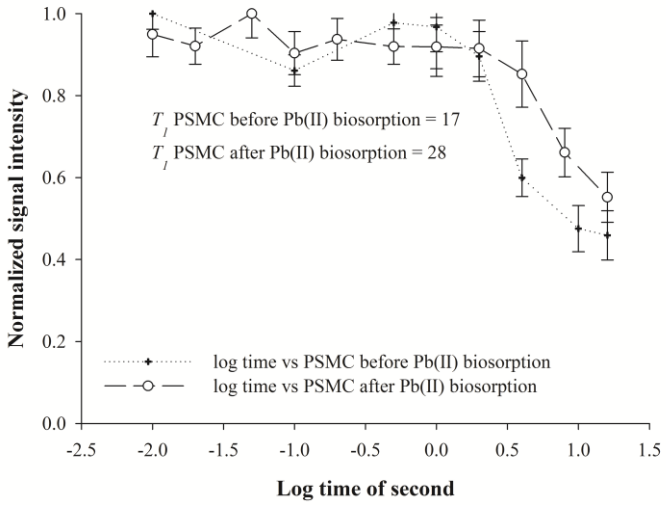

Figure 4.15 The T_1 time in TORCHIA experiments for (a) lignin carboxyl; and (b) lignin C-1/ C-4 of aromatic of syringyl and guaiacyl

Furthermore, TORCHIA experiments were conducted to differentiate the components of Pb(II) biosorption functional groups, namely, cellulose and lignin. The identified PSMC functional groups indicate that biosorptive characteristics of PSMC were attributed to lignin and not cellulose. The obtained result was in accordance to XPS and FTIR

analysis reported by Krishnani *et al*. (2008), where investigation on biomatrix from rice husk, suggested that the retention of heavy metal occurs through a complexation reaction involving carboxylate moieties of lignin or lignocellulosic.

In conclusion, SEM analysis confirmed the structure of biosorbent that established through BET surface area analysis. The relatively high amount of carbon, hydrogen, oxygen when compared to nitrogen and sulphur indicate that carbohydrate appears to be the major component of PSMC. The results of cellulose and lignin analysis further support that PSMC is a lignocellulosic biosorbent. The ^{13}C ssNMR analysis results confirmed that lignin is the component involved in heavy metal biosorption rather than cellulose. Combined results from zeta potential, XPS, FTIR and ^{13}C ssNMR indicate that weak acidic functional groups of carboxyl, hydroxyl and amide are involved in heavy metal biosorption process.

4.4.9 Pb(II) Biosorption Mechanism

Pb(II) biosorption mechanism mainly consists of ion exchange, chemisorptions and complexation. Table 4.8 summarizes the advanced characterisation methods which elucidate the functional groups involve in heavy metal biosorption mechanisms, particularly Pb(II) biosorption. The major functional groups of biosorbent were amide, hydroxyl and carboxyl which constitute potential binding sites for heavy metal ions. Details of mechanisms established through advanced characterisation are shown in Table 4.8. Discussion of these mechanisms will be highlighted in the following sections.

Table 4.8 Biosorption mechanism elucidation by functional groups determination through the use of several instrumental analysis

Mechanism	Functional groups	Supporting analysis
Ion exchange	Light metal ions of Mg(II) and Ca(II)	SEM/ EDX, XPS, ICP-OES
Chemisorptions	Hydroxyl	SEM, Zeta potential, XPS, FTIR
Complexation	Carboxyl and hydroxyl group of lignin syringyl and guaiacyl	^{13}C ssNMR
	Carboxyl group of lignin	Zeta potential, XPS, FTIR, ^{13}C ssNMR
	Amide, hydroxyl groups and O ring of N-acetylglucosamine from chitin	Zeta potential, XPS, FTIR

4.4.9.1 Ion exchange

Knowledge of Pb(II) speciation and the biosorbent surface characteristics are crucial in explaining the biosoption mechanism. As reported in Section 4.4.4 and 4.4.5, displacement of light metal ions with Pb(II) ions was supported by SEM/EDX and XPS analysis. This section provides further evidence from ICP-OES to confirm that ion exchange mechanism occur during biosorption process. Figure 4.16 shows that there was an increase in light metal ions accompanying the decrease of the Pb(II) ions.

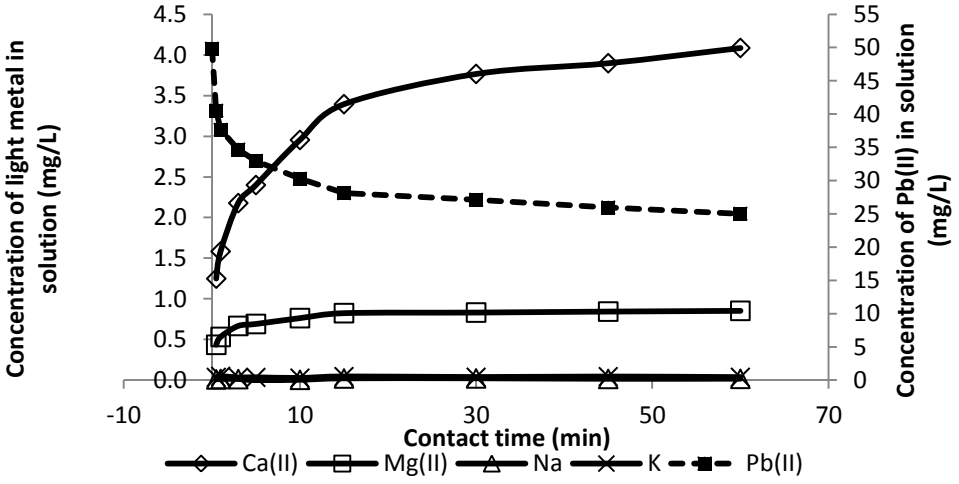

Figure 4.16 ICP-OES analysis of Pb(II) and light metal behaviour

During the biosorption process, light metal ions were released from the biosorbent which corresponded to the increase of light metal ions in the solution. Concurrently, the biosorption of Pb(II) has resulted in the decreasing of the concentration of Pb(II). These observations validated ion exchange mechanism, that metallic species of Pb(II) ions have a tendency to replace light metal ions on PSMC biosorbent. From observation, Ca(II) ions and Mg(II) ions play an important role in Pb(II) ion exchange. On the other hand, the low concentrations (0.1 - 0.2 mg/L) of Na and K indicated that ion exchange is not significant in the overall process. Therefore, it can be deduced that this ion exchange occurred according to Equations 4.1 and 4.2.

$R\text{-}Ca^{2+} + Pb^{2+} \leftrightarrow R\text{-}Pb + Ca^{2+}$ (Equation 4.1)

$R\text{-}Mg^{2+} + Pb^{2+} \leftrightarrow R\text{-}Pb + Mg^{2+}$ (Equation 4.2)

where R = matrix of the PSMC biosorbent

Similar explanation on the mechanism has also been proposed by Fiol *et al*. (2006), Vijayaraghavan *et al*. (2010), Wahab *et al*. (2010), Blázquez *et al*. (2011), Tay *et al*. (2011b) where ion exchange mechanism occur through the replacement of heavy metal with light metal. In addition, Sawalha *et al*. (2009), Li *et al*. (2011a) and Reddy *et al*. (2011) documented evidence of negligible interference by monovalent and divalent light metal in the heavy metal biosorption when heavy metal solutions contain a variety of light metal.

4.4.9.2 Chemisorptions

Several chemical bonds and ligand interactions involving hydroxyl functional group play a major role in chemisorptions. These include alcohol, sugars, some amino acids and phospholipids. Figure 4.17 shows the pH of Pb(II) solution continuously decreased

from 4.40 to 4.26 during the biosorption process. The graph showed a sudden drop of pH in the first few minutes and then gradually decreased which accompanied the Pb(II) biosorption profile.

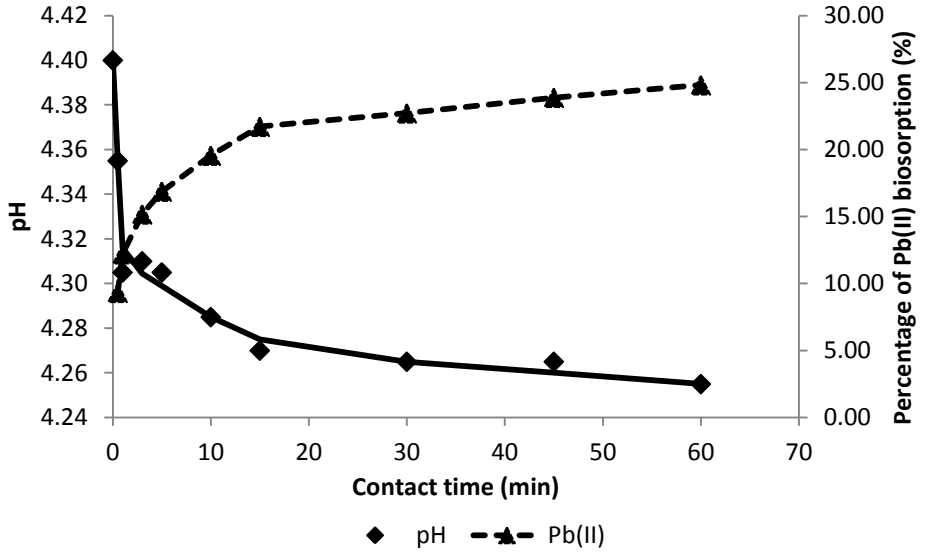

Figure 4.17 Effect of contact time on pH

This observation is attributed to protons being released into heavy metal solution from the surface of biosorbent via hydroxyl ligands. Pb(II) ions may have attached itself to two adjacent hydroxyl groups which donate two pair of electrons to the Pb(II) ion, forming two coordination number compounds and releasing two hydrogen ions into the solution. These chemisorptions mechanisms are governed by Equations 4.3 and 4.4.

$2(R\text{-}COH) + Pb^{2+} \leftrightarrow (R\text{-}CO)_2Pb + 2H^+$ (Equation 4.3)

$R\text{-}COH + Pb(OH)^+ \leftrightarrow R\text{-}CO\text{-}Pb(OH) + H^+$ (Equation 4.4)

where R = matrix of the PSMC biosorbent

A similar result on chemisorptions mechanisms was recorded for mango peel waste and lignin matrices biosorbents (Iqbal *et al*., 2009; Telysheva *et al*., 2009).

Based on the electron donating nature of the identified functional groups in the biosorbent and the electron-accepting nature of Pb(II) ions, the ion exchange

mechanism is favoured. Within the pH range of 1-5 for Pb(II) ions, there is a number of Pb(II) species present in the solution, such as Pb^{2+}, $Pb(OH)^{+}$ and $Pb(OH)_2$. The positively charged Pb(II) ions may be captured by the hydrogen bonding mechanism along with the ion exchange. The chemical bonding is a result of the sharing of a free electron pair between the surface oxygen atom and metal atom or the formation of an O-Pb(II) bond (Equation 4.5).

$$2R\text{-}COH + Pb(OH)_2 \leftrightarrow (R\text{-}COH)_2Pb(OH)_2 \quad \text{(Equation 4.5)}$$

where R = matrix of the PSMC biosorbent

Shin *et al*. (2007) and Vonodhini and Das (2009) also reported the chemisorptions-induced hydrogen bonding mechanism which is consistent with the results of this study. These chemisorptions mechanism also supported by findings from SEM in changes of biosorbent morphology after heavy metal biosorption.

4.4.9.3 Complexation

The advanced characterisation analysis elucidated that complexation mechanism only involve the lignin and chitin components. For lignin, lignin carboxyl as well as lignin syringyl and guaiacyl were identified as moieties involved in complexation. The syringyl and guaiacyl of lignin are easily oxidized by hydrogen peroxidase and laccase produce by *Pleurotus ostreatus* (Geib *et al*., 2008). Figure 4.18 shows the possible combination complexes formed by syringyl and guaiacyl of lignin with Pb(II) ions. The carbon C-1α and C-4 of syringyl and guaiacyl were implicated in complexation. The acidic groups of carboxyl and hydroxyl were predominant contributors in these lignin syringyl and guaiacyl-Pb(II) complexes.

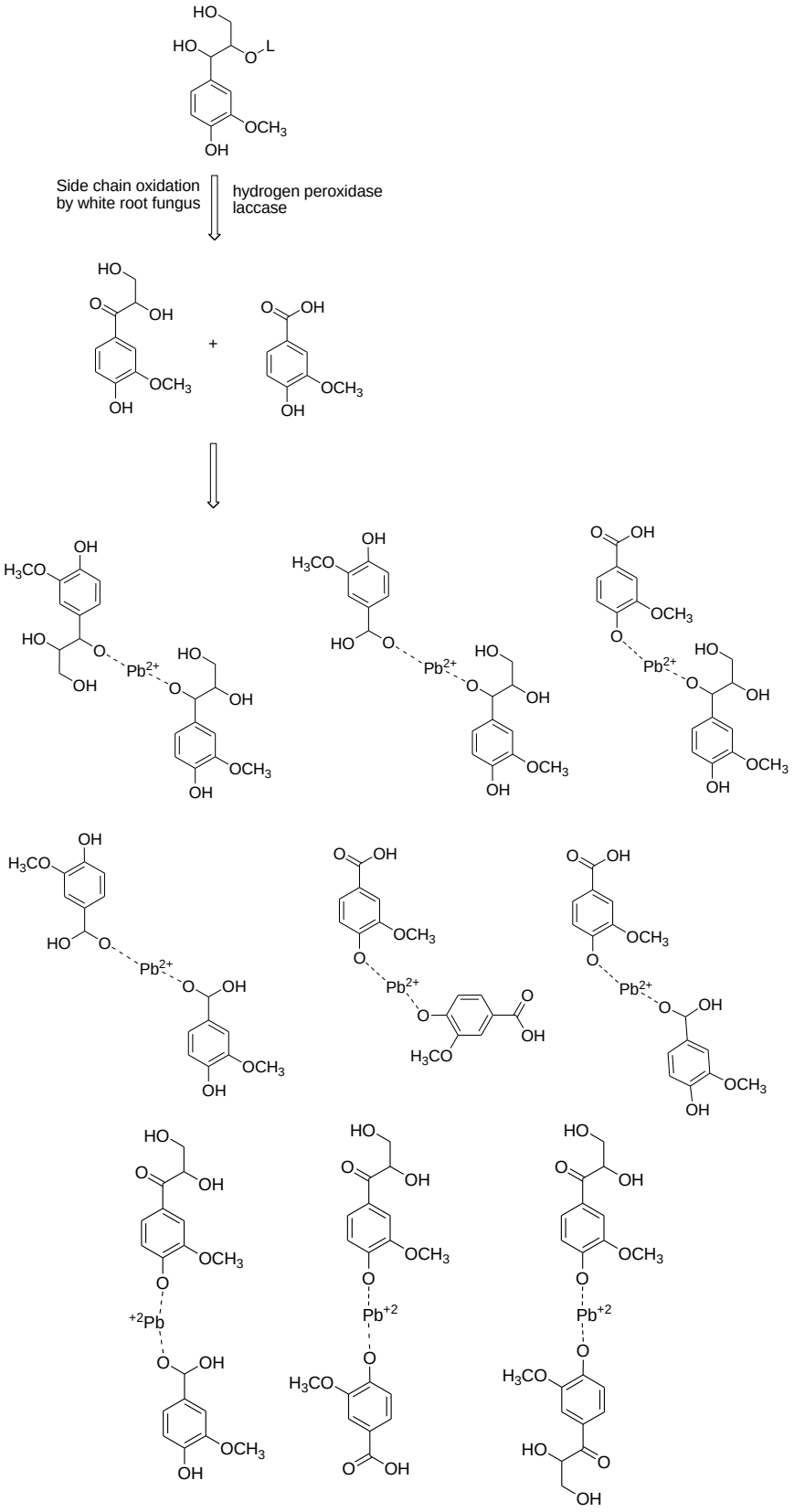

Figure 4.18 Proposed derivation of complexation structures of syringyl and guaiacyl lignin components with Pb(II) based on results of this study

The complexation formed through lignin carboxyl group, is through the bonding as shown in Figure 4.19. The lignin carboxyl group was bonded to Pb(II) ion via two oxygen atom. This mechanism was also porposed by Figueira *et al*. (1999) for carboxyl-heavy metal complex. In addition to results from XPS and FTIR analysis, this mechanism is proven through the stiffening of the C-C bond in the sample from ^{13}C ssNMR TORCHIA analysis that implies the formation of complexes between the Pb(II) and the biosorbent functional groups. Consequently, the available binding sites on the biosorbent decreased and these structural changes occurring in the biosorbent was observed through spectra shifts in XPS, FTIR and ^{13}C ssNMR.

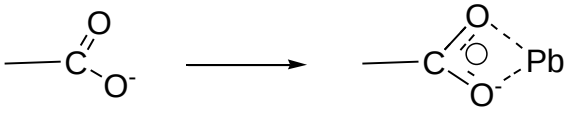

Figure 4.19 Hypothesed structure for lignin carboxyl-Pb(II) complex

Figure 4.20 illustrates the bonding formed for chitin-Pb(II) complex. The amide group, oxygen ring and hydroxyl oxygen were implicated in the complexation of heavy metal by the chitin of the fungal cell wall. It was noted that, similar findings was reported by Debbaudt *et al*. (2004) and Zhou *et al*. (2005) on the use of chitosan and cellulose/chitin beads. Evidence of this mechanism, however, comes only from the FTIR and the XPS analysis results. Lack of evidence from the ^{13}C ssNMR studies should not discount the validity of the proposed mechanism, as Bhanoori and Venkateswerlu (2000) had in their studies found that the sugar backbone of chitin does not undergo any conformational changes despite forming complexes with Cd(II). Therefore, it is not surprising that the TORCHIA experiments conducted on PSMC before and after Pb(II) biosorption in this study did not detect any changes for the sugar backbone of cellulose or chitin.

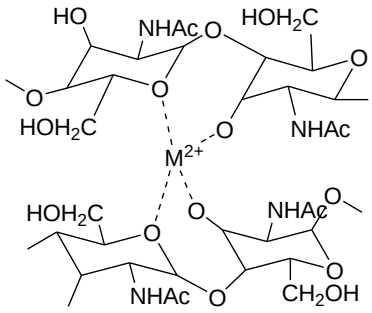

Figure 4.20 Hypothesed structure for chitin-Pb(II) complex

In summary, integrated results of SEM/EDX, zeta potential, FTIR and XPS analysis validated that ion exchange mechanism occurs in Pb(II) biosorption through replacement of light metal ions and chemisorptions mechanisms including proton release and chemical bonding of hydroxyl group. Meanwhile, the results obtained from ^{13}C ssNMR analysis, together with the results of FTIR and XPS analysis, confirmed that complexation occurs between the Pb(II) ions and the lignin carboxyl as well as carboxyl and hydroxyl functional group from lignin syringyl and guaiacyl. The FTIR results are in agreement with XPS results that complexation mechanism involves amide functional group for chitin-heavy metal complex formation.

4.5 Optimisation of Biosorption Study

Biosorbent concentration, initial pH, contact time, initial heavy metal concentration and temperature were examined in order to determine the optimum conditions for heavy metal biosorption.

4.5.1 Biosorbent Concentration

Figure 4.21 shows the effect of increasing biosorbent concentration on heavy metal biosorption. Basically, heavy metal biosorption process can be divided into three stages, namely, initial rapid stage, slow biosorption stage and equilibrium stage. In this study, only Pb(II) biosorption showed all three stages whilst the equilibrium phase for Cu(II) and Ni(II) biosorption were not observed. The Pb(II) biosorption increased from 15.26 ± 0.12 to 97.10 ± 0.07 % when biosorbent concentration was increased from 0.40 to 20.00 g/L. For the biosorption for Cu(II), an increase from 29.58 ± 0.81 to 88.91 ± 0.03 % was observed when biosorbent concentration was increased from 4.00 to 160.00 g/L. A similar trend was observed for Ni(II) with biosorption of 12.68 ± 0.17 to 88.63 ± 0.07 % when biosorbent concentration was increased from 2.00 to 160.00 g/L. At the initial rapid stage, increased in biosorbent concentration had increased the binding sites and surface area for heavy metal biosorption. Thus, this resulted in an increase of heavy metal biosorption. Following this stage, a much slower biosorption rate was observed. This is attributed to particle aggregation and coagulation of biosorbent when biosorbent concentration increased. Only Pb(II) biosorption attained the equilibrium stage which was attributed to saturation of biosorbent binding sites. Likewise, findings from studies on agricultural waste biosorbents such as pecan nutshell, *Moringa oleifera* bark, peanut shell, fungal *Mucor hiemalis* and deciduous sawdust biosorbent were found to have trends that are consistent with this study (Božić *et al*., 2009; Vaghetti *et al*., 2009; Reddy *et al*., 2010b; Shroff and Vaidya, 2011; Witek-Krowiak *et al*., 2011).

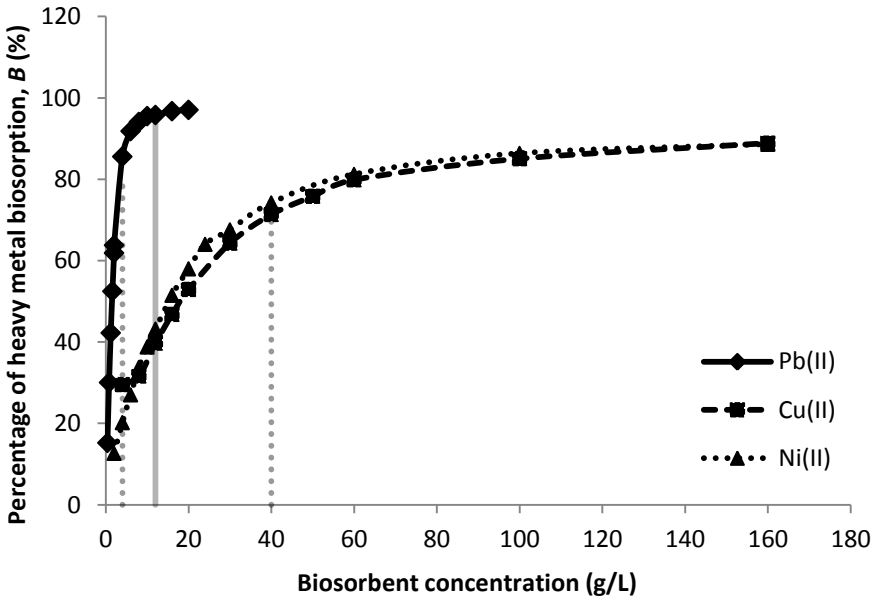

Figure 4.21 The effect of biosorbent concentration on heavy metal biosorption

As the results did not show a clear equilirium stage for Cu(II) and Ni(II) biosorption, the half saturation constant of biosorbent concentration for heavy metal biosorption was determined in order to ensure that the system is under excessive heavy metal ions condition which provides for faster reaction velocity, thus minimising the time of biosorption process and the use of biosorbent. The half saturation constant concentration was calculated via Hanes-Woolf plot, a derivation of Michaelis Menten. Table 4.9 shows the Hanes-Woolf plot equation, correlation coefficient (r^2) and the calculated half saturation constant of biosorbent concentration (K_m). The calculated half saturation constant concentration (K_m) was found to be at 0.08 g for Pb(II) biosorption while 0.7 g for both Cu(II) and Ni(II) biosorption. These established half saturation constant concentration were used in designing subsequent experiments.

Table 4.9 Hanes-Woolf plot of Michaelis Menten derivation for half saturation constant determination (K_m)

Heavy metal	Equation of Hanes-Woolf plot	r^2	K_m (g)
Pb(II)	y = 1.1680x + 0.0888	0.9956	0.08
Cu(II)	y = 1.1928x + 0.8389	0.9974	0.7
Ni(II)	y = 1.1492x + 0.8312	0.9990	0.7

4.5.2 Initial pH

Heavy metal biosorption is an initial pH dependent process as illustrated in Figure 4.22. The maximum heavy metal biosorption was found to be at 45.95 ± 1.14 %, 41.89 ± 0.31 % and 47.95 ± 0.35 % for Pb(II), Cu(II) and Ni(II) respectively, for initial pH ranging from 5 to 6. At low initial pH condition, carboxyl and hydroxyl binding sites of biosorbent are being protonated and charge repulsion occurred, thus leading to reduction in heavy metal biosorption. In addition, highly available protons also compete with heavy metal ions for binding sites on the surface of biosorbent. As initial pH increase, the binding sites are deprotonated and charge attraction is strengthened. Hence, this triggered a significant increase in heavy metal biosorption. For higher pH condition, experiments were not conducted due to precipitation of heavy metal that consequently limits the biosorption process. Furthermore, it is important to note that this result infers the recovery of heavy metal from biosorbent can be performed by acidic solutions, transferring the heavy metal which loaded in the biosorbent to the aqueous phase. Table 4.10 shows a similar order of magnitude and trend in heavy metal biosorption for plant and bacteria based biosorbents in recent studies. In subsequent experimental designs, initial pH was not adjusted since heavy metal solutions have the initial pH of 5 - 6 which correspond to the optimum range of heavy metal biosorption.

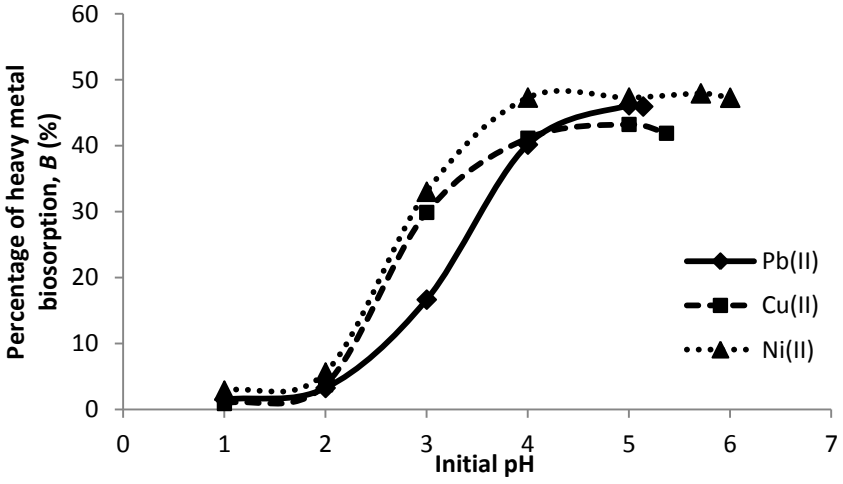

Figure 4.22 The effect of initial pH on heavy metal biosorption

Table 4.10 Comparison of initial pH at maximum heavy metal biosorption in recent studies

Heavy metal	Biosorbent	Initial pH at maximum biosorption condition	Reference(s)
Pb(II)	*Aspergillus versicolor*	5	Bairagi *et al*., 2011
	Olive tree pruning waste	5	Blázquez *et al*., 2011
	Bael leaves (*Aegle marmelos*)	5	Chakravarty *et al*., 2010b
	Garcinia mangostana L. fruit shell	5	Zein *et al*., 2010
	Chemically modified *Moringa oleifera* tree leaves	5	Reddy *et al*., 2010a
	Chemically modified corncobs	5	Tan *et al*., 2010
	PSMC	**5**	**This study**
Cu(II)	Fungus *Trametes versicolor*	5	Subbaiah *et al*., 2011a
	Peanut shell	5	Witek-Krowiak *et al*., 2011
	Fungus *Agaricus bisporus*	5	Ertugay and Bayhan, 2010
	Chemically modified pine cone powder	5	Ofomaja and Naidoo, 2010
	Marine brown algae *Laminaria japonica*	4.3-6.5	Liu *et al*., 2009
	PSMC	**5**	**This study**
Ni(II)	*Moringa oleifera* bark	6	Reddy *et al*., 2011
	Barley straw	4.85	Thevannan *et al*., 2010
	Acacia leucocephala bark	5	Subbaiah *et al*., 2009
	Bacteria *Rhodococcus opacus*	5	Cayllahua *et al*., 2009
	Bacteria *Pseudomonas* sp. and *Staphylococcus xylosus*	5-6	Gialamouidis *et al*., 2009
	PSMC	**5-6**	**This study**

4.5.3 Contact Time

Figure 4.23 depicts a familiar three phase heavy metal biosorption process, initially a rapid increase phase, slow biosorption phase and then followed by an equilibrium phase. The equilibrium phase for Pb(II) biosorption was found to be at 50.18 ± 0.53 %, which was attained within 90 minutes. Meanwhile, biosorption of Cu(II) and Ni(II) achieved equilibrium phase at 39.54 ± 0.64 % and 45.16 ± 0.64 % within 10 minutes, respectively. This indicates that binding sites at external surface of biosorbent were easily occupied by heavy metal ions, thus leading to significant increase of heavy metal biosorption at the initial phase. The biosorption process later became slower as heavy metal need to diffuse into the internal surface when external binding sites were progressively covered by heavy metal ions. The equilibrium phase was ascribed to saturation of binding sites of biosorbent. From the perspective of biosorption mechanism, physical adsorption and ion exchange occur in initial rapid biosorption phase, followed by complexation at slow biosorption phase and finally binding sites saturation condition at equilibrium phase.

Studies listed in Table 4.11 also shows a similar trend of observation for heavy metal biosorption process, whereby starting with a high rate followed by a slow biosorption phase and finally the equilibrium phase where no significant changes with further increase in contact time was observed. In addition, Table 4.11 shows that contact time of heavy metal biosorption using biosorbent concentrations corresponded to the half saturation constant are comparable to other researchers. It should be noted that the other researchers utilized biosorbent concentration at equilibrium phase or random selection under various operating conditions. By applying the half saturation constant approach in heavy metal biosorption, the equilibrium time could be achieved rapidly. The rapid heavy metal biosorption is highly desirable for use of the PSMC biosorbent in practical

applications. It is a main criterion for economical and effective heavy metal treatment. Based on this result, subsequent experiments were conducted under equilibrium phase within short period of contact time, i.e., 90 minutes for Pb(II) biosorption and 10 minutes for both Cu(II) and Ni(II) biosorption.

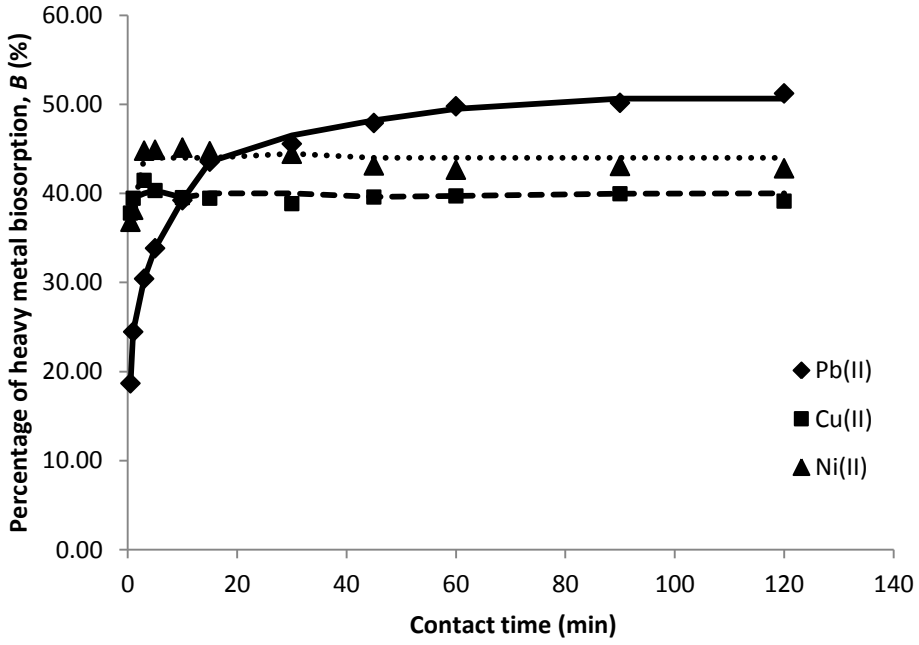

Figure 4.23 The effect of contact time on heavy metal biosorption

Table 4.11 Comparison of contact time on heavy metal biosorption

Heavy metal	Biosorbent	Contact time at equilibrium phase (min)	Conditions (weight of biosorbent, volume and concentration of heavy metal)	Reference(s)
Pb(II)	Red algae *Gymnogongrus torulosa*	360	0.1 g, 100 mL, 73 mg/L	Areco and dos Santos Afonso, 2010
	Acacia leucocephala bark	180	0.6 g, 100 mL, 100 mg/L	Munagapati *et al*., 2010
	Fungus *Mucor indicus*	120	0.05 g, 75 mL, 10 mg/L	Javanbakht *et al*., 2011
	Green algae *Enteromorpha prolifera*	60	0.05 g, 100 mL, 40 mg/L	Li *et al*., 2011b
	PSMC	**90**	**0.08 g, 50 mL, 50 mg/L**	**This study**
Cu(II)	*Cassia angustifolia* tree bark	120	1 g, 100 mL, 3 mg/L	Meena *et al*., 2008
	Algae, moss, sawdust	60	0.2 g, 100 mL, 10 mg/L	Grimm *et al*., 2008
	Treated leave powder	90	0.05 g, 25 mL, 50 mg/L	Kilic *et al*., 2009
	Baker's yeast	15-20	0.1 g, 100 mL, 25 mg/L	Zhang *et al*., 2010
	Peanut shell	60	0.1 g, 200 mL, 100 mg/L	Witek-Krowiak *et al*., 2011
	PSMC	**10**	**0.7 g, 50 mL, 50 mg/L**	**This study**
Ni(II)	*Acacia leucocephala* bark	120	0.1 g, 100 mL, 50 mg/L	Subbaiah *et al*., 2009
	Moringa oleifera bark	60	0.2 g, 50 mL, 50 mg/L	Reddy *et al*. 2011
	Fungus *Mucor hiemalis*	150	0.05 g, 10 mL, 50 mg/L	Shroff and Vaidya, 2011
	PSMC	**10**	**0.7 g, 50 mL, 50 mg/L**	**This study**

4.5.4 Initial Heavy Metal Concentration

The effect of initial heavy metal concentration on heavy metal biosorption is shown in Figure 4.24. The biosorption of heavy metal decreased as initial heavy metal concentration was increased. When initial heavy metal concentration was increased from 10 to 60 mg/L, biosorption of Pb(II), Cu(II) and Ni(II) decreased from 83.81 ± 0.49 % to 48.02 ± 1.53 %, 52.78 ± 1.22 % to 40.22 ± 0.35 % and 67.71 ± 0.89 % to 4.39 ± 0.37 % respectively. Generally, initial heavy metal concentration provides a driving force between aqueous and solid phases to overcome mass transfer resistance. The increase of initial heavy metal concentration has led to the reduction of available binding sites. As a result, a lower collision between biosorbent and heavy metal ions has resulted in reduction of heavy metal biosorption. Similar trend of Pb(II) biosorption was observed by Nadeem *et al*. (2009), Rao *et al*. (2010) and Javanbakht *et al*. (2011) where chemically modified chickpea *Cicer arientinum*, egg shell and fungus *Mucor indicus* were utilized as biosorbents. Likewise, Bhatti *et al*. (2009) and Pehlivan *et al*. (2009b) reported consistent trend in Cu(II) biosorption using flower distillation sludge and barley straw. A similar trend of observation involving Ni(II) biosorption studies using maple sawdust and tea waste were documented by Malkoc and Nuhoglu (2005) and Shukla *et al*. (2005) respectively. Having such results, the PSMC is highly potential for the purification of diluted heavy metal contaminated wastewater.

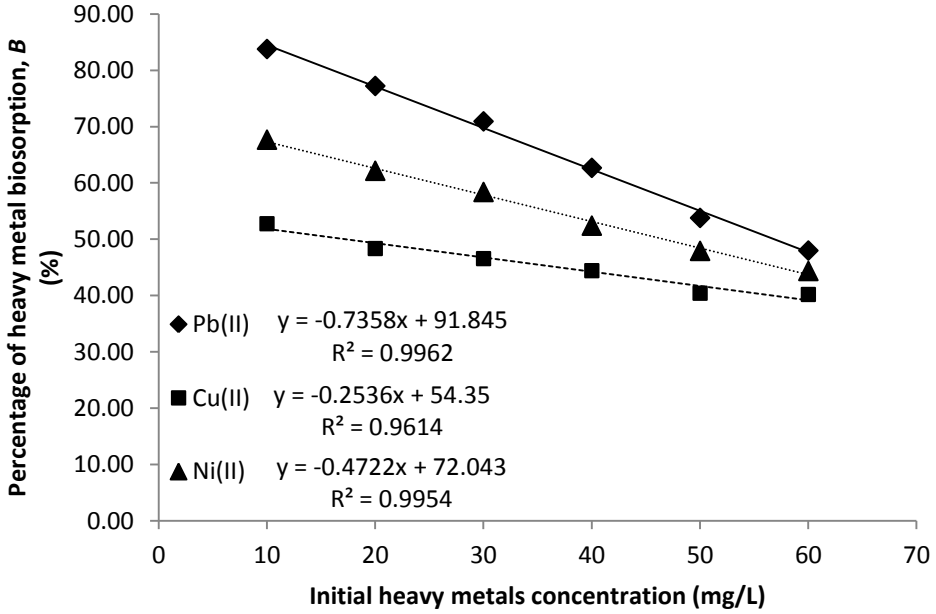

Figure 4.24 The effect of initial heavy metal concentration on heavy metal biosorption

4.5.5 Temperature

Figure 4.25 illustrates the effect of temperature on heavy metal biosorption, examined at four different temperatures. Heavy metal biosorption decreased slightly, within 10 %, when temperature was increased by 20 ^{o}C. As the temperature increased in the range of 5 to 35 ^{o}C, heavy metal biosorption decreased linearly from 89.37 ± 0.76 % to 79.26 ± 0.10 %, 58.56 ± 0.20 % to 52.56 ± 1.00 % and 74.03 ± 0.17 % to 67.18 ± 0.40 % for Pb(II), Cu(II) and Ni(II) respectively. The increase of temperature may cause greater diffusion process and better driving force. However, it did not increase the heavy metal biosorption process. This suggests that heavy metal biosorpion process is an exothermic reaction. Exothermic reactions have difficulties in releasing energy to the environment when there is an increase in environmental temperature, thus causing decrease of heavy metal biosorption. Nevertheless, this result needs to be investigated and supported by biosorption thermodynamic parameters. It was observed that a similar trend for temperature profile in heavy metal biosorption was reported by Arslanoglu *et al*. (2009), Areco and dos Santos Afonso (2010) and Mulgund *et al*. (2011) on the use of esterified

lemon, red algae *Gymnogongrus torulosa* and *Cassia angustifolia* bark as biosorbent respectively.

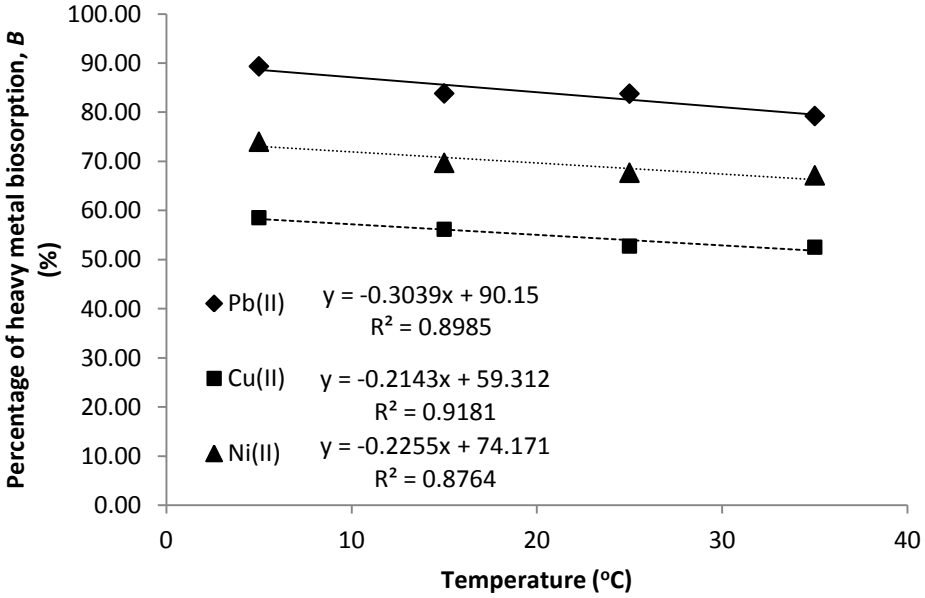

Figure 4.25 The effect of temperature on heavy metal biosorption

4.6 Selectivity of Heavy Metal Biosorption

Table 4.12(a-c) compares the selectivity of PSMC biosorbent in single heavy metal, bi-heavy metal and multi-heavy metal. The heavy metal selectivity order of the PSMC biosorbent in single heavy metal biosorption was similar to bi-heavy metal and multi-heavy metal biosorption. Biosorbent exhibited highest heavy metal selectivity towards Pb(II), followed by Ni(II) and lastly Cu(II). This result corresponded to the decrease of electronegativity of heavy metal. The electronegativity of Pb, Ni and Cu are 2.33, 1.91 and 1.90 Pauling scale respectively. It can be deduced that the electronegavity reflects the selectivity of heavy metal biosorption. Similar results on higher selectivity towards Pb(II) than Cu(II) were obtained in Otero *et al*. (2009), Vijayaraghavan *et al*. (2009), Cao *et al*. (2010) and Chatterjee *et al*. (2010) where studies were performed using biosorbents from sewage sludge, marine brown algae *Sargassum* sp. immobilised spent fungus *Tricholoma lobayense*, and bacteria *Geobacillus thermodenitrificans* respectively. However, the observed Cu(II) has the lowest selectivity when compared to

Pb(II) and Ni(II). This finding is in contradiction with that reported by Božić *et al*. (2009). Božić *et al*. (2009) documented that the ranking sequence was Cu(II) higher than Ni(II) for decidous tree sawdust without any description and justification. Consistent observation among the selectivity of heavy metal in single, bi- and multi-heavy metal in this study is important for biosorbent application in industrial wastewater containing multi-heavy metal ions.

Table 4.12(a) Percentage of single heavy metal biosorption for investigated parameters

Single heavy metal selectivity	Parameters	Heavy metal biosorption, *B* (%)		
		Pb(II) at 0.08 g	Cu(II) at 0.7 g	Ni(II) at 0.7 g
Pb(II) > Ni(II) > Cu(II)	The established half saturation constant concentration of biosorbent	50.00	50.00	50.00
	Initial pH 5 - 6	45.95 ± 1.14	41.89 ± 0.31	47.95 ± 0.35
	Contact time at 120 minutes	50.18 ± 0.53	39.54 ± 0.64	45.16 ± 0.64
	The calculated initial heavy metal concentration at 50 mg/L from Figure 4.13	55.06	41.67	48.43

Table 4.12(b) Percentage of bi-heavy metal biosorption for investigated parameters

Bi-heavy metal	Parameters	Heavy metal biosorption, *B* (%)		
		Pb(II)	Cu(II)	Ni(II)
Pb(II)Cu(II) at 0.08 g	Initial pH 5 - 6	48.65 ± 0.77	14.05 ± 0.40	-
Selectivity:	Contact time at 120 minutes	45.62 ± 2.72	11.79 ± 0.10	-
Pb(II) >Cu(II)	Initial heavy metal concentration, ratio 1:1	39.49 ± 0.76	11.69 ± 0.22	-
Pb(II)Ni(II) at 0.08 g	Initial pH 5 - 6	64.11 ± 1.23	-	6.88 ± 0.70
Selectivity:	Contact time at 120 minutes	60.74 ± 0.10	-	1.47 ± 0.38
Pb(II) >Ni(II)	Initial heavy metal concentration, ratio 1:1	44.06 ± 6.61	-	8.24 ± 1.61
Pb(II)Cu(II) at 0.7 g	Initial pH 5 - 6	96.27 ± 0.04	45.06 ± 0.47	-
Selectivity:	Contact time at 120 minutes	95.94 ± 0.52	42.67 ± 2.36	-
Pb(II) >Cu(II)	Initial heavy metal concentration, ratio 1:1	94.58 ± 0.24	44.38 ± 0.49	-
Pb(II)Ni(II) at 0.7 g	Initial pH 5 - 6	96.07 ± 0.09	-	53.87 ± 0.09
Selectivity:	Contact time at 120 minutes	96.43 ± 0.19	-	52.81 ± 3.84
Pb(II) >Ni(II)	Initial heavy metal concentration, ratio 1:1	95.24 ± 0.57	-	56.12 ± 0.40
Cu(II)Ni(II) at 0.7 g	Initial pH 5 - 6	-	43.99 ± 0.64	47.10 ± 0.14
Selectivity:	Contact time at 120 minutes	-	40.46 ± 0.74	43.45 ± 0.92
Ni(II) >Cu(II)	Initial heavy metal concentration, ratio 1:1	-	42.75 ± 1.74	47.63 ± 0.72

- Not applicable

Table 4.12(c) Percentage of multi-heavy metal biosorption for investigated parameters

Multi-heavy metal	Parameters	Heavy metal biosorption, *B* (%)		
		Pb(II)	Cu(II)	Ni(II)
Pb(II)Cu(II)Ni(II) at 0.7 g	Initial pH 5 – 6	96.83 ± 0.39	48.13 ± 0.48	52.93 ± 0.05
	Contact time at 120 minutes	96.13 ± 0.53	41.07 ± 0.26	47.17 ± 0.40
Selectivity: *Pb(II) > Ni(II) > Cu(II)*	Initial heavy metal concentration, ratio 1:1:1	94.73 ± 0.31	47.04 ± 0.52	53.56 ± 1.07

In short, optimisation and selectivity of heavy metal biosorption was examined. The half saturation constant concentration was found at 0.08 g for Pb(II) and 0.7 g for both Cu(II) and Ni(II). Initial pH of heavy metal solutions at un-adjusted pH, represented the optimum heavy metal biosorption condition. Pb(II) biosorption process reached equilibrium phase within 90 minutes of contact time whilst both Cu(II) and Ni(II) achieved equilibrium phase within 10 minutes of contact time. Heavy metal biosorption is dependent on initial heavy metal concentration, but slightly influenced by temperature. The PSMC biosorbent showed highest selectivity towards Pb(II), followed by Ni(II) and finally Cu(II). The heavy metal selectivity order is similar and consistent for single heavy metal, bi-heavy metal and multi-heavy metal biosorption. Hence, the new approach of using the half saturation constant concentration not only minimise operating time and use of biosorbent but also leads to more reliable results as the limitation and operating conditions are under controlled.

4.7 Evaluation of Existing Mathematical Models

Result from single heavy metal biosorption was evaluated using existing models, namely, Langmuir isotherm, pseudo first-order kinetic, pseudo second-order kinetic and thermodynamic.

4.7.1 Langmuir Isotherm Model

The Langmuir isotherm model is well established for monolayer biosorption on the surface of biosorbent. Table 4.13 shows that heavy metal biosorption using PSMC biosorbent was excellently fitted to Langmuir isotherm. The correlation coefficient of Pb(II), Cu(II) and Ni(II) were 0.9988, 0.9695 and 0.9983 respectively. Results specifically point out that heavy metal biosorption occurred in a single layer, involving interaction of heavy metal ions with functional groups on the surface of PSMC biosorbent.

Table 4.13 The Langmuir isotherm parameters for heavy metal biosorption using PSMC biosorbent

Heavy metal	q_{max} (mg/g)	b (L/mg)	r^2
Pb(II)	21.10	0.1696	0.9988
Cu(II)	3.87	0.0218	0.9695
Ni(II)	3.03	0.0573	0.9983

Table 4.13 also shows that the calculated maximum uptake for heavy metal (q_{max}) were found to be at 21.10 mg/g, 3.87 mg/g and 3.03 mg/g for Pb(II), Cu(II) and Ni(II) respectively. These constitute evidences that PSMC biosorbent is a promising biosorbent for treating wastewater containing heavy metal since PSMC is relatively abundant and effective. The PSMC biosorbent has highest q_{max} for Pb(II), followed by Cu(II) and lastly Ni(II). Heavy metal with high atomic number, standard atomic weight and atomic radius radii exhibit a better capacity in q_{max}. Likewise, Zakhama *et al*. (2011) reported that algae *Ulva lactuca* has q_{max} value in descending order for Pb(II),

Cd(II), Cu(II) and Ni(II). Furthermore, results from studies using chemically modified orange peel, green algae and cork waste biosorbents also are consistent with this finding where Pb(II) remarkably showed highest q_{max} when compared to Cd(II), Cu(II) or Ni(II) (Feng *et al*., 2011; Lee and Chang, 2011; López-Mesas *et al*., 2011; Lasheen *et al*., 2012). Observations where q_{max} for Cu(II) is higher than Ni(II) was also documented by Kleinübing *et al*. (2012).

Taking the Langmuir constant (*b*) into consideration, the PSMC biosorbent demonstrates an obvious selectivity towards Pb(II) at 0.1696 L/mg when compared to 0.0573 L/mg for Ni(II) and 0.0218 L/mg for Cu(II). The result infers that the parameter *b* for Pb(II) is approximate one order of magnitude higher than Cu(II) and Ni(II). The parameter *b* of heavy metal biosorption strengthened results from the established half saturation constant concentration and selectivity of heavy metal biosorption discussed in Section 4.5.1 and 4.6 respectively. Such desirable circumstance leads to effective treatment of the targeted heavy metal in industrial wastewater.

Table 4.14(a-c) compares the parameters of PSMC Langmuir isotherm heavy metal biosorption with that of the different biosorbents cited in the recent literature. The PSMC biosorbent has a comparable q_{max} when compared to other raw biosorbents with the exception of fungus *Agaricus cerevisiae* for Cu(II) as well as bacteria *Rhodococcus opacus* and waste pomace of olive oil factory for Ni(II). These can be attributed to the fine particle size of 104 µm for fungus *Agaricus cerevisiae* and 150-250 µm of waste pomace. The fine particles give higher surface area when compared to 710 µm of PSMC biosorbent. The fine particle sizes of biosorbents increase the surface area and thus resulted in improvement of q_{max}.

Additionally, the lower q_{max} values for PSMC biosorbent when compared to modified or high containing light metal ions biosorbents are shown in Table 4.14. To improve the q_{max} values of a particular biosorbent, many researchers utilised both chemical and heat modifications. Although these modifications may substantially improve the q_{max} values, a severe shortcoming in many of these modified biosorbents is the lack of an environment impact carbon footprint assessment of the modifications on the biosorbents. The impact of chemical and heat modification may very well diminish the sustainablility value of reusing agricultural waste as an environmentally friendly biosorbent. On the other hand, algae, moss and Ca-alginate based biosorbents are rich in light metal ions such as Ca(II), Mg(II), Na and K (Stokke *et al*., 2000; Reimann *et al*., 2001; Davis *et al*., 2003). This circumstance favours the ion exchange mechanism. Hence, a better performance in heavy metal biosorption was documented.

Table 4.14(a) Comparison of Pb(II) Langmuir isotherm parameters with other recent studies using PSMC biosorbent

Biosorbent	Langmuir parameters q_{max} (mg/g), [mmol/g]	Langmuir parameters b (L/mg), [L/mmol]	r^2	Reference(s)
Raw biosorbents				
Walnut sawdust	15.90	0.01	0.9558	Bulut and Tez, 2007
Spent fungal corncob based substrate	14.75	0.0007	0.7417	Jonglertjunya, 2008
Fungus *Pleurotus ostreatus*	14.75	0.0873	0.9496	Tay *et al*., 2009
Shell of hazelnut *Corylus avellana* and almond *Prunus dulcis*	28.18, 8.08 [0.136, 0.039]	4.1752, 0.3441 [865.052, 71.304]	0.981, 0.982	Pehlivan *et al*., 2009a
Crushed de-oiled residue of allspice (*Pimenta dioica* L. Merrill)	12.09	0.468	0.995	Cruz-Olivares *et al*., 2011
Fungus *Mucor indicus* for mostly filamentous, purely filamentous, purely yeast-like and mostly yeast-like	15.63, 22.07, 12.12, 14.68	0.069, 0.187, 0.077, 0.1142	0.9986, 0.9968, 0.9936, 0.9998	Javanbakht *et al*., 2011
PSMC	**21.10**	**0.1696**	**0.9988**	**This study**
Modified biosorbents				
Formaldehyde treated Meranti tree sawdust	37.04	0.02	0.97	Ahmad *et al*., 2009
Chemically treated rubber leaf powder (*Hevea brasiliensis*)	95.3	2.2	0.996	Kamal *et al*., 2010
Highly contain light metal ions biosorbents				
P. ostreatus immobilized in calcium alginate bead	121.21	0.0046	0.9456	Xiangliang *et al*., 2005
Chitosan beads, chitosan-glutaraldehyde beads, chitosan-alginate beads	34.98, 14.24, 60.27	0.000076, 0.000018, 0.00025	0.9575, 0.9717, 0.9177	Ngah and Fatinathan, 2010

Table 4.13(b) Comparison of Cu(II) Langmuir isotherm parameters with other recent studies using PSMC biosorbent

Biosorbent	Langmuir parameters q_{max} (mg/g), [mmol/g]	Langmuir parameters b (L/mg), [L/mmol]	r^2	Reference(s)
Raw biosorbents				
Rice husk	2.48	0.143	0.996	Ong *et al*., 2007
Sawdust from birch wood *Betula* sp.	4.9	0.20	-	Grimm *et al*., 2008
Spent fungal corncob based substrate	1.77	0.0007	0.8816	Jonglertjunya, 2008
Yeast *Saccharomyces cerevisiae*	2.595	0.07466	0.994	Cojocaru *et al*., 2009
Fungus *Agaricus bisporus*	9.1157	0.0241	0.9294	Ertugay and Bayhan, 2010
Pleurotus ostreatus	3.6	0.0154	0.9927	Tay *et al*., 2010
PSMC	**3.87**	**0.0218**	**0.9695**	**This study**
Modified biosorbents				
HNO_3 treated rice husk	9.36	0.080	0.994	Ong *et al*., 2007
NaOH treated rubber leaves powder (*Hevea brasiliensis*)	14.97	0.412	0.9962	Ngah and Hanafiah, 2008
NaOH treated wheat straw *Triticum aestivum*	11.44 [0.18]	0.0301 [1.91]	0.92	Dang *et al*., 2009
H_3PO_4 treated rubberwood sawdust	5.55	2.874	0.9982	Kalavathy *et al*., 2009
Formaldehyde treated Meranti tree sawdust	37.17	0.07	0.95	Ahmad *et al*., 2009
Formaldehyde and NaOH treated mangrove bark	5.8038	0.0271	0.9364	Rozaini *et al*., 2010
Highly contain light metal ions biosorbents				
Marine brown algae *Fucus vesiculosus*, terrestrial moss *Pleurozium schreberi*,	23.4, 11.1,	1.01, 1.15,	-	Grimm *et al*., 2008
Fungus *Pycnoporus sanguineus* immobilized Ca-alginate beads	2.962	1.168	1.000	Yahaya *et al*., 2009

Table 4.14(c) Comparison of Ni(II) Langmuir isotherm parameters with other recent studies using PSMC biosorbent

Biosorbent	Langmuir parameters q_{max} (mg/g), [mmol/g]	Langmuir parameters b (L/mg), [L/mmol]	r^2	Reference(s)
Raw biosorbents				
Walnut sawdust	3.29	0.01	0.9754	Bulut & Tez, 2007
Industrial raw kraft lignin	3.79 [0.0646]	0.9548 [56.04]	0.978	Betancur *et al*., 2009
Bacteria *Rhodococcus opacus*	7.621	0.254	0.95	Cayllahua *et al*., 2009
Waste pomace of olive oil factory	10.64	0.0475	0.982	Nuhoglu and Malkoc, 2009
PSMC	**3.03**	**0.0573**	**0.9983**	**This study**
Modified biosorbents				
Demineralised kraft lignin	9.17 [0.1562]	0.7047 [41.36]	0.965	Betancur *et al*., 2009
Heat treated *Moringa oleifera* bark	26.84	0.26	-	Reddy *et al*., 2011
Chemically pre-treated brown algae *Laminaria japonica*	15.26-66.32 [0.26-1.13]	0.0167, 0.0290 [0.98-1.70]	0.954 -0.989	Liu *et al*., 2009
HCl treated algae (*Oedogonium hatei*)	44.247	0.063	0.982	Gupta *et al*., 2010
Highly contain light metal ions biosorbents				
Phaseolus vulgaris L. entrapped in silica-gel matrix	98.02 [1.67]	0.00004 [2.12×10^3]	0.999	Akar *et al*., 2009
Untreated algae (*Oedogonium hatei*)	40.983	0.06	0.985	Gupta *et al*., 2010

- Not available

4.7.2 Pseudo First-order and Second-order Kinetic Models

The pseudo first-order and second-order kinetic models were used to investigate kinetic in biosorption process in order to gain insight into biosorption mechanism and rate controlling factor. Table 4.15 shows heavy metal biosorption fitted better to pseudo second-order kinetic when compared to pseudo first-order kinetic. The measurement of fitness for kinetic models is made through the correlation coefficient and experimental value of heavy metal uptake at equilibrium phase (q_e). The pseudo first-order kinetic plots correlation coefficients are not satisfactory (< 0.99) and the calculated q_e do not matched the experimental q_e. Results infer that heavy metal biosorption on PSMC is not uni-molecular reaction, thus biosorption does not occur exclusively onto one site per ion. Similarly, lower calculated values of q_e compared to experimental values were also reported by Feng *et al*. (2009).

On the other hand, the heavy metal biosorption excellently fitted to pseudo second-order kinetic model as high values of the correlation coefficients were obtained and experimental q_e were in excellent agreement with the calculated values. This strongly suggests that the rate of heavy metal biosorption appears to be limited by chemisorptions, through the formation of chemical bonds. The results indicate that heavy metal biosorption is complex involving several mechanisms occurring simultaneously.

Nuhoglu and Malkoc (2009), Areco and dos Santos Afonso (2010) and Wahab *et al*. (2010) not only documented results which well fitted to pseudo second-order kinetic compared to first-order kinetic, but also suggested that chemisorptions are the rate limiting factor in heavy metal biosorption for waste pomace, marine algae *Gymnogongrus torulosus* and *Eucalyptus globulus* sawdust biosorbents.

Table 4.15 Pseudo first-order and second-order parameters for three heavy metal biosorption using PSMC biosorbent

Heavy metal	Pseudo first-order kinetic			Experimental q_e	Pseudo second-order kinetic		
	q_e	k_1	r^2		q_e	k_2	r^2
Pb(II)	5.20	0.0389	0.8054	15.26	15.46	0.0184	0.9994
Cu(II)	0.05	0.0085	0.3242	1.47	1.45	3.1214	0.9999
Ni(II)	0.06	0.0518	0.1432	1.64	1.62	11.0594	0.9999

4.7.3 Thermodynamic Model

The orientation and feasibility of the physicochemical biosorption reaction can be evaluated through the parameters in thermodynamic study. Thermodynamic parameters, namely, free energy (ΔG), enthalpy changes (ΔH) and enthropy changes (ΔS) are shown in Table 4.16. In general, the value of ΔG increased slightly with increasing temperature, indicating that the heavy metal biosorption process would become less favourable when temperature rises. These results indicate that heavy metal biosorption is mainly a physical rather than chemical in nature. The negative value of ΔG suggested the spontaneous nature of heavy metal biosorption and the degree of spontaneity of the reaction slightly decreased with increasing of temperature. The negative value of ΔH signified the exothermic reaction for heavy metal biosorption. This conforms to the findings from temperature profiles where heavy metal biosorption is exothermic in nature. The negative ΔS value represented weaker and reversible bonds were formed after biosorption process. This implies that the PSMC biosorbent has a good potential for heavy metal recovery from biosorbent. However, this assumption needs to be confirmed by recovery of heavy metal from biosorbent in application study which will be discussed further in 4.8.2. Similar results were found in biosorbent such as fungus *Mucor rouxii*, fungus *Agarican bisporus* and chemically modified marine algae *Cystoseira stricta* (Ertugay and Bayhan, 2010; Majumdar *et al*., 2010; Iddou *et al*., 2011). In most cases, sawdust biosorbents only reported similar result where heavy

metal biosorption is a sponteneous reaction (Bulut and Tez, 2007; Meena *et al*., 2008; Naiya *et al*, 2009).

Table 4.16 Thermodynamic parameters for heavy metal biosorption utilizing PSMC biosorbent

Heavy metal	Temperature (K)	ΔH (kJ/ mol)	ΔS (kJ/ mol/ K)	ΔG (kJ/ mol)	r^2
Pb(II)	278	-4717	-0.04	-4705	0.8888
	288			-4704	
	298			-4704	
	308			-4703	
Cu(II)	278	-1733	-0.02	-1728	0.9301
	288			-1727	
	298			-1727	
	308			-1727	
Ni(II)	278	-2178	-0.02	-2172	0.8871
	288			-2172	
	298			-2172	
	308			-2172	

In summary, the heavy metal biosorption using PSMC biosorbent well fitted to Langmuir isotherm model which suggest a monolayer biosorption system. The PSMC biosorbent is a suitable biosorbent since it has comparable q_{max} value with other biosorbents. Meanwhile, the parameter *b* indicates that the PSMC biosorbent is effective in targeted heavy metal treatment. Kinetics models assist in biosorption mechanism explanation and biosorption limiting factor. Heavy metal biosorption better fitted to pseudo second-order kinetic than first-order. This indicates that the heavy metal biosorption is not a uni-molecular reaction where heavy metal ions bind to more than one binding sites. Chemisorptions contribute in rate limiting factor and several mechanisms may occur simultaneously during heavy metal biosorption. Thermodynamic model offers description of orientation and feasibility reaction nature.

Heavy metal biosorption using PSMC biosorbent is a spontaneous, exothermic and reversible reaction. These results not only explain the heavy metal biosorption process system and mechanism, but also provide basic information for biosorption application study in following section.

4.8 Application of Biosorbent

In biosorbent application study, biosorbent performance in treatment of automobile wastewater together with recovery of heavy metal from biosorbent was investigated.

4.8.1 Biosorbent Performance in Treatment of Automobile Wastewater Containing Ni(II)

The automobile wastewater containing Ni(II) was selected in application study as the current heavy metal treatment method using chemical precipitation is not effective and costly especially when concentration of Ni(II) is higher than 10 mg/L and generates large volume of toxic sludge. The results of heavy metal biosorption from automobile wastewater are shown in Table 4.17. In addition, Table 4.17 also shows the comparison between Ni(II) biosorption in automobile wastewater with calculated Ni(II) biosorption in Ni(II) solution which was presented earlier in Figure 4.24. Generally, the Ni(II) biosorption in treatment of automobile wastewater was lower when compared to calculated Ni(II) biosorption from Figure 4.24. This may be attributed to the presence of other heavy metal such as manganese (Mn) and zinc (Zn) in automobile wastewater which compete for similar binding sites on the surface of the biosorbent. Besides, concentration of each heavy metal and species of heavy metal ions in automobile wastewater also may influence the heavy metal biosorption. Furthermore, the initial pH of biosorption process in automobile wastewater was lower than the optimum initial pH for biosorption, being at pH 3.75 - 4.02. Protons competed with selected heavy metal ions for binding sites, thus reducing the efficiency of selected heavy metal biosorption. It can be deduced that the PSMC biosorbent is a potential biosorbent to treat industrial wastewater containing heavy metal. Similar observation was reported by Akar *et al*. (2009) and Javaid *et al*. (2011) where fungus *Aspergillus flavus* and fungus *Pleurotus ostreatus* biosorbents were applied in treating industrial wastewater respectively.

Table 4.17 Heavy metal biosorption in five different automobile wastewater samples using PSMC biosorbent

n pH	Heavy metal	Before biosorption (mg/L)			After biosorption (mg/L)			Heavy metal biosorption (%)				Calculated Ni(II) biosorption from Fig. 4.24
		1	2	average	1	2	average	1	2	average	std. dev.	y = -0.4722x + 72.043
1	Cu	-	-	-	-	-	-	-	-	-	-	
3.75	Mn	7.9230	7.8630	7.8930	5.1570	5.1800	5.1685	34.91	34.12	34.52	0.56	
	Ni	15.6300	15.5100	15.5700	8.2540	8.2440	8.2490	47.19	46.85	47.02	0.24	64.69
	Pb	-	-	-	-	-	-	-	-	-	-	
	Zn	11.3700	11.3300	11.3500	5.1410	5.1350	5.1380	54.78	54.68	54.73	0.08	
2	Cu	-	-	-	-	-	-	-	-	-	-	
3.82	Mn	6.3140	6.3660	6.3400	3.7930	3.8130	3.8030	39.93	40.10	40.02	0.12	
	Ni	12.5200	12.6200	12.5700	6.0490	6.0020	6.0255	51.69	52.44	52.06	0.53	66.11
	Pb	-	-	-	-	-	-	-	-	-	-	
	Zn	8.5620	8.5650	8.5635	3.4810	3.4810	3.4810	59.34	59.36	59.35	0.01	
3	Cu	-	-	-	-	-	-	-	-	-	-	
3.79	Mn	5.7870	5.7610	5.7740	3.2890	3.3380	3.3135	43.17	42.06	42.61	0.78	
	Ni	11.7500	11.6100	11.6800	5.3600	5.5430	5.4515	54.38	52.26	53.32	1.50	66.53
	Pb	-	-	-	-	-	-	-	-	-	-	
	Zn	6.5630	6.4910	6.5270	2.4420	2.5370	2.4895	62.79	60.92	61.85	1.33	

4	Cu	-	-	-	-	-	-	-	-	-	-	
4.02	Mn	4.7200	4.6910	4.7055	2.7160	2.4800	2.5980	42.46	47.13	44.80	3.31	
	Ni	9.3890	9.3340	9.3615	4.5870	4.0920	4.3395	51.14	56.16	53.65	3.55	67.62
	Pb	-	-	-	-	-	-	-	-	-	-	
	Zn	5.7970	5.7720	5.7845	2.2880	2.0050	2.1465	60.53	65.26	62.90	3.35	
5	Cu	-	-	-	-	-	-	-	-	-	-	
3.91	Mn	5.6770	5.6520	5.6645	3.3970	3.4330	3.4150	40.16	39.26	39.71	0.64	
	Ni	10.6700	10.6200	10.6450	5.1990	5.2820	5.2405	51.27	50.26	50.77	0.71	67.02
	Pb	-	-	-	-	-	-	-	-	-	-	
	Zn	8.3350	8.2970	8.3160	3.3840	3.4630	3.4235	59.40	58.26	58.83	0.80	

- Not present

4.8.2 Recovery of Heavy Metal from Biosorbent

Figure 4.26 shows the schematic diagram of mass balance for biosorption-desorption cycle. Overall, the mass balance before and after desorption was in good agreement. The mass balance before desorption (W_b + C_b) for Pb(II), Cu(II) and Ni(II) were 81.6290 ± 0.0643 mg, 668.0205 ± 0.0134 mg and 701.2505 ± 0.1442 mg respectively. Meanwhile, the mass balance after desorption (W_d + C_d) were 74.5971 ± 1.9275 mg for Pb(II), 622.7795 ± 8.4612 mg for Cu(II) and 660.8136 ± 7.7231 mg for Ni(II). The loss after desorption (W_l + C_l) for Pb(II), Cu(II) and Ni(II) were 7.0319 ± 1.9918 mg, 45.2410 ± 8.4478 mg and 40.4369 ± 7.8673 mg respectively. The percentages of loss in mass balance for all heavy metal were less than 10 %.

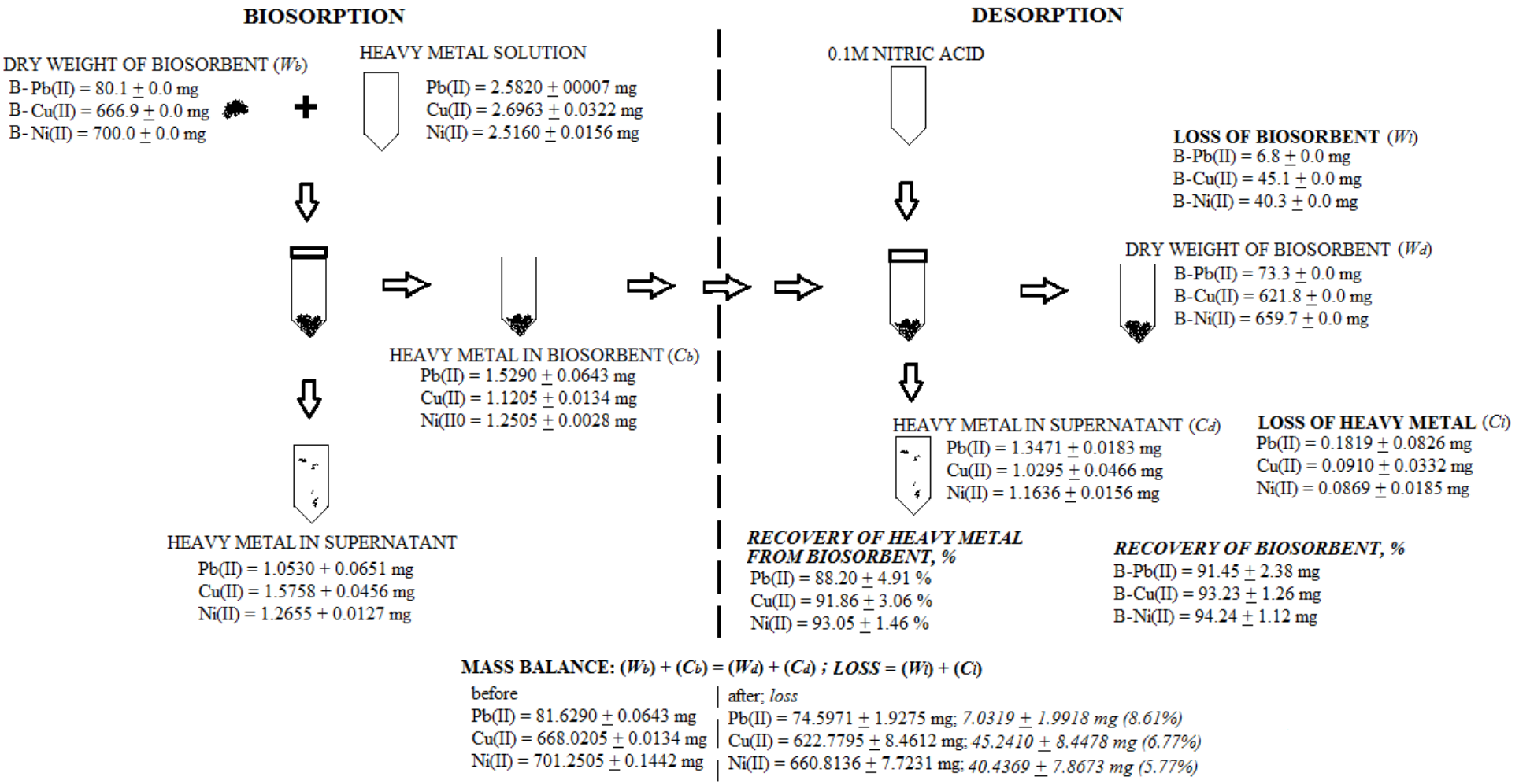

Figure 4.26 Schematic diagram of biosorption-desorption process for mass balance and recovery

As shown in Figure 4.26, Pb(II) after desorption (C_d) was found to be 1.3471 ± 0.0183 mg in 0.1M nitric acid compared to 1.5290 ± 0.0643 mg Pb(II) in biosorbent before desorption (C_b). For Cu(II), an amount of 1.0295 ± 0.0466 mg was measured in 0.1M nitric acid (C_d) compared to 1.1205 ± 0.0134 mg Cu(II) in biosorbent before desorption (C_b). A similar profile was observed for Ni(II) of 1.1636 ± 0.0156 mg in 0.1M nitric acid (C_d) from 1.2505 ± 0.0028 mg Ni(II) in biosorbent before desorption (C_b). Hence, the percentage of heavy metal recovery for Pb(II), Cu(II) and Ni(II) were attained at 88.20 ± 4.91 %, 91.86 ± 3.06 % and 93.05 ± 1.46 %. The weight loss of heavy metal were 0.1819 ± 0.0826 mg for Pb(II), 0.0910 ± 0.0332 mg for Cu(II) and 0.0869 ± 0.0185 mg for Ni(II). One of the possible reasons of approximately 90 % heavy metal recovery and heavy metal weight loss may be due to the loss of biosorbent laden with heavy metal during the transfer of supernatant. The capillary action trapped the residue heavy metal between the biosorbent particles. The subsequent washing steps washed off the trapped heavy metal and hence caused the loss of heavy metal before desorption. These losses of heavy metal are inevitable and should be accounted as heavy metal loss indicated as (C_l) in Figure 4.26.

The biosorbent weight loss and recovery after biosorption-desorption cycle was considered in this study. This approach has not been reported in the literature except by Mata *et al*. (2010). As shown in Figure 4.26, the dry weight of biosorbent for Pb(II), Cu(II) and Ni(II) before (W_b) and after (W_d) biosorption-desorption cycle were 73.3 ± 0.0 mg and 80.1 ± 0.0 mg, 621.8 ± 0.0 mg and 666.9 ± 0.0 mg as well as 659.7 ± 0.0 mg and 700.0 mg respectively. Results for recovery of biosorbent were 91.45 ± 2.38 % for Pb(II), 93.23 ± 1.26 % for Cu(II) and 94.24 ± 1.12 % for Ni(II). The biosorbent loss (W_l) during the biosorption-desorption cycle were found to be 6.8 ± 0.0 mg for Pb(II), 45.1 ± 0.0 mg for Cu(II) and 40.3 ± 0.0 mg for Ni(II). The weight loss of biosorbent

after the biosorption-desorption cycle can be caused by the centrifugation and removal of the supernatant for heavy metal detection in which some fine heavy metal loaded biosorbent particles were removed together with the supernatant. Hence, the percentage of biosorbent recovery is reduced.

In short, desorption process using 0.1M nitric acid has successfully eluted the heavy metal from biosorbent with high recovery percentage and low weight loss. Both biosorption and desorption results also support the findings from initial pH in optimisation study in Section 4.5.2 and enthropy changes (ΔS) in thermodynamic model in Section 4.7.3 where reversible bonding is formed after biosorption and then heavy metal can be easily eluted by dilute acids.

Table 4.18 shows that the PSMC has higher percentage heavy metal recovery from biosorbent compared to other biosorbents. Thus, the disposal of other biosorbents can become a problem as there are still small quantities of heavy metal within the biosorbent. Since the heavy metal are considered fully recovered from the PSMC biosorbent as seen from the accounted mass balance, it can be safely disposed after desorption or converted to biochar or vermicomposted to return the carbon back to the environment. This reveals that the biodegradable PSMC biosorbent and heavy metal in dilute acid can be recycled, extracted or used in downstream industries, thus minimising waste as well as the negative environmental impact.

Table 4.18 Comparison study for recovery percentage and desorption parameters of this study with those recently reported in literature

Biosorbent	Heavy metal	Elution acid	Recovery (%)	Reference(s)
Bacteria *Pseudomonas* sp. and *Staphylococcus xylosus*	Ni(II)	0.1M HNO_3	87	Gialamouidis *et al*., 2009
Barley straw	Cu(II)	0.1M HCl	75-80	Pehlivan *et al*., 2009b
Ficus religiosa leaves	Pb(II)	0.05M HNO_3	88	Qaiser *et al*., 2009
Fungus *Rhizopus cohnii*	Cd(II)	0.1M HCl	98.8	Luo *et al*., 2010
Fungus *Aspergillus versicolor*	Pb(II)	0.1M HCl	85	Bairagi *et al*., 2011
Fungus *Mucor indicus*	Pb(II)	0.05M HNO_3	88	Javanbakht *et al*., 2011
Moringa oleifera bark	Ni(II)	0.2M HCl	92.08	Reddy *et al*., 2011
PSMC	**Pb(II), Cu(II), Ni(II)**	**0.1M HNO_3**	**88.20, 91.86, 93.05**	**This study**

In summary, the heavy metal biosorption in automobile wastewater is always lower than that in synthetic single heavy metal solution. Competition for the binding sites occurred between the selected heavy metal with protons or other heavy metal in the wastewater. Furthermore, each heavy metal concentration and species in wastewater as well as pH of wastewater affects the performance of the PSMC biosorbent in heavy metal biosorption. For heavy metal biosorption-desorption cycle, an approximately 90 % recovery for both heavy metal and biosorbent were observed. The loss of heavy metal and biosorbent can be attributed to the fine particles loaded with heavy metal being removed together with the supernatant during biosorption-desorption cycle. Furthermore, the washing steps after biosorption washed off the trapped heavy metal between biosorbent particles and resulted in loss of heavy metal. Results from biosorbent application study indicate that the PSMC bioosrbent is a suitable biosorbent for heavy metal treatment in industrial wastewater. Besides that, the high recovery of heavy metal from biosorbent with accounted mass balance reveals that biosorbent generates less secondary products and can be disposed off safely. This study also provides fundamental information which can be used for column and pilot scale study.

4.9 Artificial Neural Network (ANN) Modelling

The ANN model development involved three activities, namely, ANN structure development, ANN structure optimisation and sensitivity analysis (Maier and Dandy, 2000).

4.9.1 ANN Structure Development

Figure 4.27 illustrates MATLAB script where commands for loading and scaling input data were employed. The training data set included all the data in the problem domain to update the weights of the network. The input was scaled to 0 to 1 with the aim to match the nonlinear function employed for the hidden neurons.

```
%load input data
x=load('Ni(II)trainInputs.m'); % input patterns
allx=load('Ni(II)AllInputs.m'); % all input patterns = training + test
data
maxx=max(allx);maxx=max(maxx); % preprocess by scaling, since 'net
function' using sigmoidal
x1=x/maxx;
y=load('Ni(II)trainTargets.m'); % targets
ally=load('Ni(II)AllTargets.m');
maxo=max(ally);maxo=max(maxo);
out_target=y/maxo;
x1=x1';
y1=out_target';
```

Figure 4.27 MATLAB script – loading and scaling input data

Basically, the developed ANN structure is a feed forward network with a back propagation training algorithm, a tangent sigmoid transfer function at the hidden layer and a linear transfer function at the output layer. In the preliminary assessment of the ANN structure, a single hidden layer was adopted. This allows for the rapid evaluation of the output, namely, s.s.e and m.s.e values as well as the correlation coefficient. For the overall architecture of the ANN, initial training parameters were set as in the script shown in Figure 4.28. The last instruction in Figure 4.28 was to train the network.

```
%initialise training matrix
%network parameters
net=newff(minmax(x1),[1,3],{'tansig','purelin'},'trainlm');
net.trainParam.show = 10;
net.trainParam.lr = 0.9;
net.trainParam.lr_inc = 0.001;
net.trainParam.mc = 0.7;
net.trainParam.epochs = 1000;
net.trainParam.goal = 0.00001;
[net,tr]=train(net,x1,y1);
```

Figure 4.28 MATLAB script – setting training parameters

As shown in Figure 4.29, the equation $y = 0.9911x$ with correlation coefficient of 0.9798 was obtained when trained data was compared to prediction data. In addition, low error values of 1.52×10^{-3} m.s.e and 1.64×10^{-1} s.s.e were attained for this trained ANN structure. Based on the low m.s.e and s.s.e values as well as the high correlation coefficient, the ANN structure is deemed as a suitable ANN structure for subsequent optimisation process.

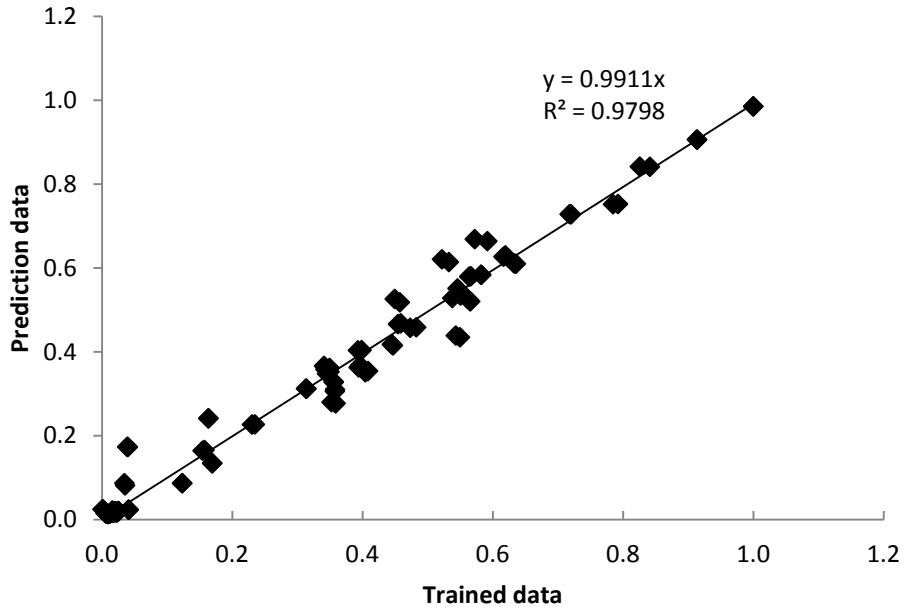

Figure 4.29 Predictions of ANN with developed ANN model compared to trained data

4.9.2 ANN Structure Optimisation

Three optimisation parameters, namely, hidden layer, learning rate and momentum rate were examined to optimise the ANN model. The hidden layer determines the number and arrangement of connection weights. Meanwhile, the learning rate is directly proportional to the size of the steps taken in weight space and thus optimal learning rates are determined by trial and error. The momentum rate is considered to speed up the training process by several orders and magnitude.

4.9.2.1 Hidden layer

Figure 4.30 and 4.31 depict the ANN training errors of m.s.e and s.s.e for different hidden layer size. Hidden layer of 10 recorded the lowest error values, 6.86 x 10^{-6} m.s.e and 7.41 x 10^{-4} s.s.e. Performance goal at hidden layer of 10 was met with number of epochs at 124/ 1000. The equation for hidden layer of 10 was found to be $y = 0.9987x$ with correlation coefficient of 0.9999. Comparison on before and after hidden layer of 10, found no significant changes on m.s.e and s.s.e. values due to under fitting and over fitting of hidden layer respectively. For economic and time saving reasons, the developed ANN model with hidden layer 10 was selected for final application.

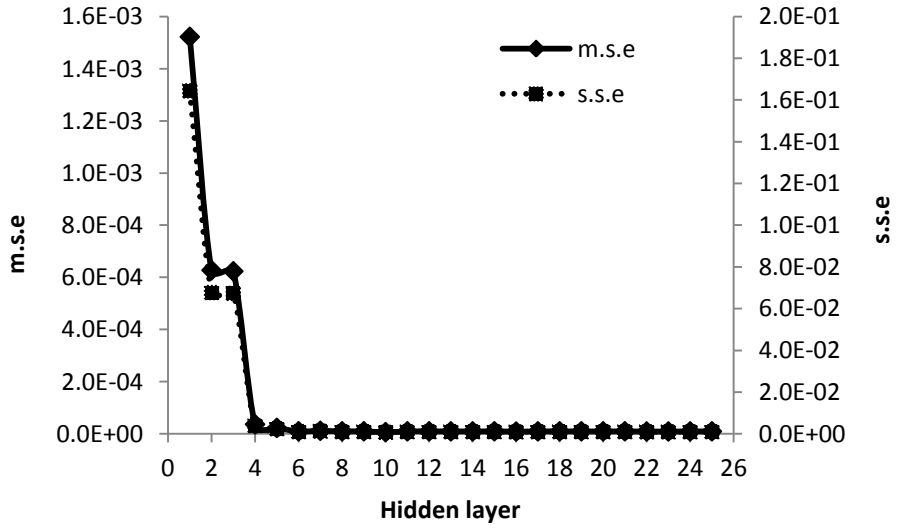

Figure 4.30 Results obtained from ANN training showing the errors with varying hidden layer size

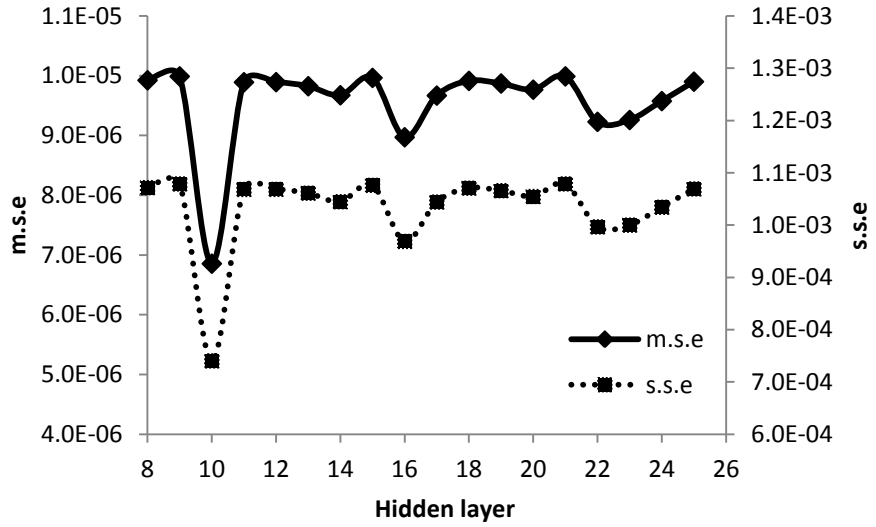

Figure 4.31 Results obtained from ANN training showing the errors for hidden layer 8 to 25

4.9.2.2 Learning rate

Figure 4.32 shows the ANN training m.s.e and s.s.e for different learning rate. The learning rate with minimum errors was attained at 0.6 where m.s.e and s.s.e were 8.25 x 10^{-6} and 8.91 x 10^{-4} respectively. At 0.6 learning rate, the equation of $y = 1.0003x$ with correlation coefficient of 0.9999 was obtained and the performance goal was met with 44/ 1000 epochs. Hence, learning rate of 0.6 was selected for final application.

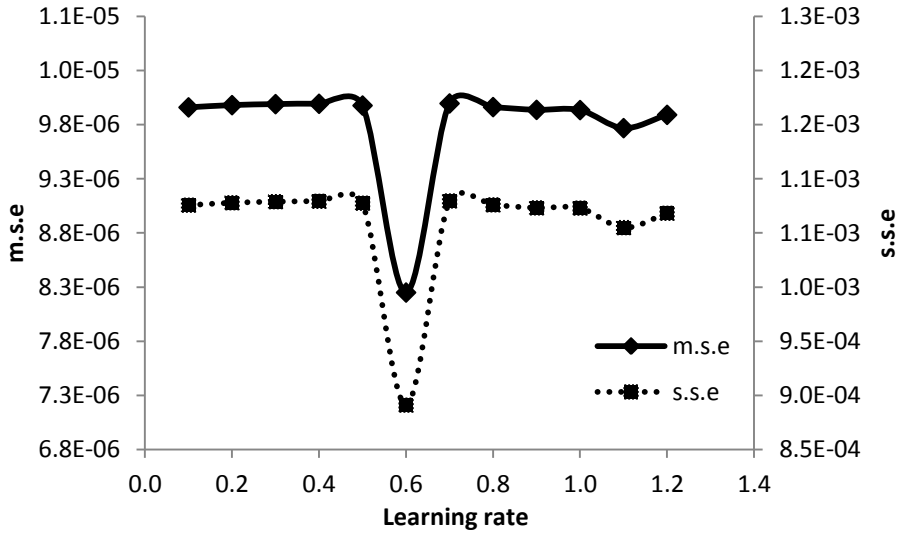

Figure 4.32 Results obtained from ANN training showing the errors with varying learning rate size

4.9.2.3 Momentum rate

The ANN training data errors for different momentum rate is shown in Figure 4.33. The minimum errors were found to be at momentum rate of 0.6. The minimum m.s.e of 8.25 x 10^{-6} and s.s.e of 8.91 x 10^{-4} were recorded. Excellent equation and correlation coefficient were $y = 1.0003x$ and 0.9999 respectively. The performance goal was met at number of epochs at 44/1000. Based on minimum errors, excellent equation and high correlation coefficient, the momentum rate of 0.6 was selected for final application.

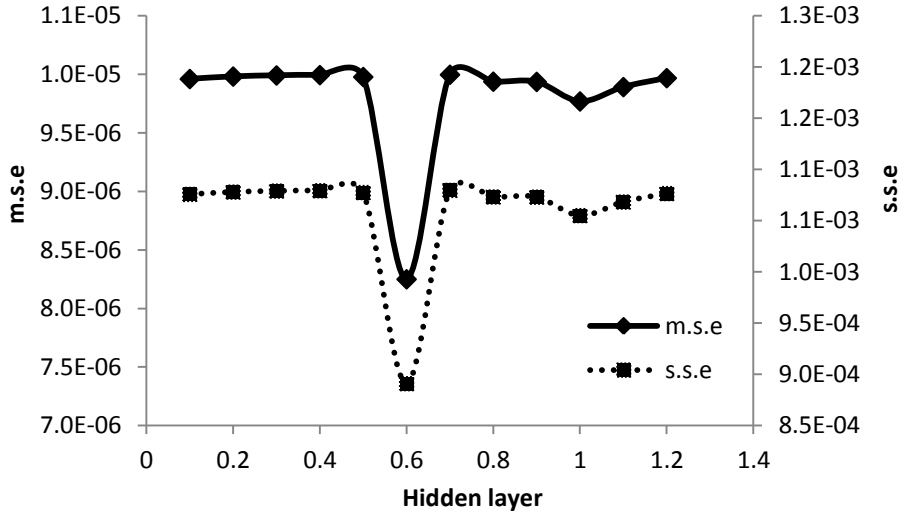

Figure 4.33 Results obtained from ANN training showing the errors with varying momentum rate

4.9.3 Sensitivity Analysis

Figure 4.34 illustrates that results of predicted data obtained through the network simulation for training data set and testing data set, are in close agreement with experimental data. The best linear equation and coefficient value were found to be $y = 0.9998x$ and 0.9750 respectively. The errors values were 1.46 x 10^{-3} for m.s.e and 1.58 x 10^{-1} for s.s.e. Therefore, the developed and optimised ANN model is reliable and accurate in multiple output prediction.

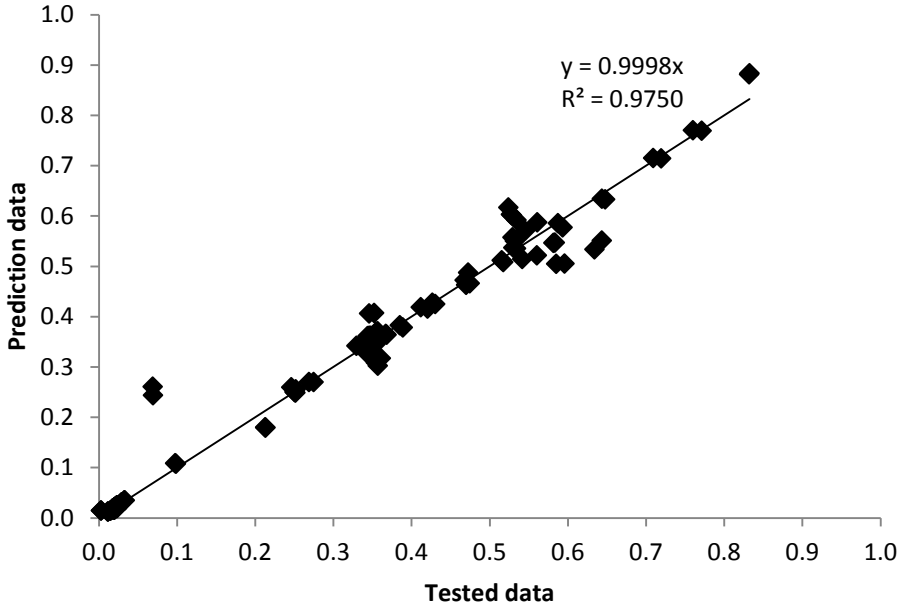

Figure 4.34 Comparison between the experimental values and the predicted values using developed ANN model

Table 4.19 shows the comparison of the developed ANN model for heavy metal biosorption with other researchers. To date, there is no literature on more than one output ANN model in heavy metal biosorption. Thus, this developed multiple output Ni(II) biosorption ANN model is a knowledge contribution in biosorption technology, especially for industrial or pilot application. Furthermore, such multiple output ANN model is crucial in determining water quality of effluent and the most suitable time for elution of biosorbent or shutdown of plant operation.

Table 4.19 Comparison study for application of the developed ANN model with other ANN models in heavy metal biosorption using biosorbent

Constructed ANN model	Input	Output	Validation performance	Biosorbent	Heavy metal	Reference
Back-propagation Recurrent Network, momentum-training algorithm, Tanh and linear sigmoid transfer function	4	1	The ultimate m.s.e was found to be 2.139579×10^{-3} which is within ±1%	*Mangifera indica* sawdust	Cu(II)	Prakash *et al*., 2008
A three-layer Back-propagation combined with principal component analysis network, Levenberg-Marquardt algorithm, *tansig* and *purelin* function	5	1	Minimum m.s.e and correlation coefficient were 2.27875×10^{-4} and 0.936 respectively	Antep pistachio (*Pistacia vera* L.) shell	Pb(II)	Yetilmezsoy and Demirel, 2008
A two-layer Back-propagation Feed Forward network, Levenberg-Marquardt algorithm, Sigmoid transfer function	4	1	Minimum m.s.e was 3.707393×10^{-3}	Shelled *Moringa Oleifera* seed powder	Cd(II)	Kardam *et al*., 2010
A single-layer Back-propabation feed Forward Network, , Levenberg-Marquardt algorithm, Sigmoid transfer function	4	1	Minimum m.s.e was 8.665268×10^{-3}	Shelled *Moringa Oleifera* seed powder	Ni(II)	Raj *et al*., 2010
A single-layer Back-propagation Feed Forward Network, Levenberg-Marquardt algorithm, *tansig* and *purelin* function	**4**	**3**	**The testing data with equation of $y = 0.9998x$, $r^2 = 0.9750$, m.s.e = 1.48×10^{-3}, s.s.e = 1.58×10^{-1}**	**PSMC**	**Ni(II)**	**This study**

In conclusion, a multiple output ANN model was developed. This ANN architecture involves a feedforward network with back propagation training algorithm, tangent sigmoid transfer function at hidden layer and a linear transfer function at output layer. The optimal structure of the developed and optimised ANN model, which is based on minimum m.s.e and s.s.e values, was determined at hidden layer of 10, learning rate of 0.6 and momentum rate of 0.6. This developed network has a good ability to predict the response of experimental data through sensitivity analysis with equation $y = 0.9998x$, $r^2 = 0.9750$, m.s.e of 1.46×10^{-3} and s.s.e of 1.58×10^{-1}. The developed ANN model not only enhanced the modelling knowledge on biosorption process but also has the potential to contribute in operation management and effluent quality monitoring through multiple prediction output.

4.10 Concluding Remarks

Experiments conducted according to methodology described in Chapter III have yielded results on:

i. The novel reporting and evaluation of the washing pre-treatment approach in biosorbent preparation is a vital study in order to remove contaminants and enhance heavy metal biosorption. Excellent reproducibility and repeatability observed in these studies also indicate that the methodology adopted was good.

ii. Advanced characterisation of biosorbent elucidated biosorption mechanisms. From the analysis of integrated results, ion exchange, chemisorptions and complexation are identified as the main mechanisms in heavy metal biosorption, particularly for Pb(II). A novel approach of using ^{13}C ssNMR TORCHIA experimental design is applied in biosorbent advanced characterisation. This new approach successfully confirmed the complexation mechanism involving lignin guaiacyl and syringyl with Pb(II) ions.

iii. In the optimisation study, the half saturation constant concentration for heavy metal biosorption in synthetic heavy metal solutions was introduced. This approach successfully minimised the biosorption operational time and biosorbent usage in order to obtain reliable results under controlled conditions.

iv. Selectivity of biosorbent towards heavy metal followed the order of Pb(II), Ni(II) and Cu(II) which corresponded to the electronegativity in descending order. The selectivity of biosorbent is consistent for single heavy metal, bi-heavy metal and multi-heavy metal solutions.

v. Evaluation of existing models involved Langmuir isotherm, pseudo first-order kinetic, pseudo second-order kinetic and thermodynamic. These evaluations shed light to spontaneous exothermic, not uni-molecular monolayer heavy metal biosorption system and reversible bonding formed after biosorption. In existing

models evaluation, chemisorptions are characterised by monolayer and exothermic system. Chemisorptions are mechanisms that also act as the rate limiting factor in heavy metal biosorption process. Several mechanisms may occur simultaneously during heavy metal biosorption process.

vi. Biosorbent performance in treatment of automobile wastewater containing Ni(II) was lower when compared to synthetic Ni(II) solution. Competition for binding sites between targeted heavy metal ions with other heavy metal and protons resulted in lower biosorption efficiency. In addition, heavy metal biosorption was also influenced by initial heavy metal concentration and species of heavy metal in wastewater.

vii. High recovery of heavy metal from biosorbent at approximately 90% infers that heavy metal can easily be eluted from biosorbent by dilute acid In addition, it reduced secondary waste products. Hence, it is a sustainable biosorbent for heavy metal treatment.

viii. A novel multiple output ANN model was developed for heavy metal biosorption. This new approach assists planning and decision making for plant management and effluent quality monitoring.